

# Multiscale change point detection via gradual bandwidth adjustment in moving sum processes

Tijana Levajković and Michael Messer\*

Vienna University of Technology

## Abstract

A method for the detection of changes in the expectation in univariate sequences is provided. Moving sum processes are studied. These rely on the selection of a tuning bandwidth. Here, a framework to overcome bandwidth selection is presented – the bandwidth adjusts gradually. For that, moving sum processes are made dependent on both time and the bandwidth: the domain becomes a triangle. On the triangle, paths are constructed which systematically lead to change points. An algorithm is provided that estimates change points by subsequent consideration of paths. Strong consistency for the number and location of change points is shown. Simulations support estimation precision. A companion R-package `mscp` is made available on CRAN.

Keywords: *change point detection, moving sum, multiscale, gradual bandwidth, mscp*.  
MSC subject classifications: 62G20, 62M99.

## 1 Introduction

We contribute to the field of change point detection in stochastic sequences. Change point detection applies in various research areas, e.g., climatology (Reeves et al., 2007), speech recognition (Rybach et al., 2009), oceanography (Killick et al., 2010), neuroimaging (Aston and Kirch, 2012), virology (Kass-Hout et al., 2012) etc.

We consider  $T$  univariate and independent random variables (RVs)  $X_1, \dots, X_T$ , that are piecewise identically distributed, with existing  $(2 + p)$ -th moments ( $p > 0$ ), without parametric assumptions. Multiple change points in expectation form a set  $C$ . See Figure 1 (bottom) for an example with  $T = 200$ ,  $X_i \sim N(\mu, \sigma^2)$ , three change points  $C = \{65, 105, 145\}$ , and thus four sections with parameters  $\mu = 1, 4, 1, -2$  and  $\sigma = 1, 0.8, 1, 0.5$ , i.e., changes in  $\sigma$  may additionally occur when  $\mu$  changes.

There is extensive literature that covers changes in expectation, e.g., methods based on likelihood ratios (Gombay and Horváth, 1994; Fang et al., 2020), empirical processes (Horváth and Shao, 2007; Holmes et al., 2013),  $U$ -statistics (Gombay and Horváth, 2002; Horváth and Hušková, 2005; Döring, 2010), least-squares (Lavielle and Moulines, 2000; Harchaoui and Lévy-Leduc, 2010) and many more. We mention methodology based

---

\*corresponding author

on CUSUM-statistics, e.g., by Page (1954); Hinkley (1971); Berkes et al. (2006); Dehling et al. (2017). For a general overview of change point methods see the textbooks of Csörgő and Horváth (1997); Chen and Gupta (2000); Brodsky (2017). In this paper, we aim to tackle multiple change points that may occur on different time scales, as considered e.g., in Spokoiny (2009); Fryzlewicz (2014); Matteson and James (2014); Pein et al. (2017).

We study moving sum processes (MOSUM), see e.g., Chu et al. (1995); Steinebach and Eastwood (1995); Antoch and Hušková (1999); Hušková and Slabý (2001). For that we select a window size (bandwidth)  $h \in \{1, \dots, \lfloor T/2 \rfloor\}$  and define MOSUM  $(D_{t,h})_t$  for index  $t = h, \dots, T - h$ : for every time  $t$  consider two adjacent windows of size  $h$ , left  $\{t - h + 1, \dots, t\}$  (index  $\ell$ ) and right  $\{t + 1, \dots, t + h\}$  (index  $r$ ), and set

$$D_{t,h} := \sqrt{h} \cdot \frac{\hat{\mu}_r - \hat{\mu}_\ell}{(\hat{\sigma}_r^2 + \hat{\sigma}_\ell^2)^{1/2}} \quad (1)$$

where  $\hat{\mu}_j$  and  $\hat{\sigma}_j^2$  denote the mean and empirical variance of the RVs whose indices lie in the windows,  $j \in \{\ell, r\}$ .  $D_{t,h}$  is Welch's  $t$ -statistic for two samples of size  $h$ . We typically find  $|D_{t,h}| \approx 0$  if no change is involved, but  $|D_{t,h}| > 0$  if there is a change nearby,  $t \approx c \in C$ . Thus, change point estimates may be obtained by argmax-estimation, see e.g., Eichinger and Kirch (2018).

A major challenge lies in the choice of the window size  $h$ . An  $h$  small enough is sensitive to rapid changes when it does not overlap subsequent change points, while a larger  $h$  improves detection power of small effects as more RVs are evaluated. But note that  $h$  too large may result in overlap of subsequent changes and thus in an estimation bias. In order to account for change points that occur on multiple time scales, including rapid changes as well as small effects, methods that combine multiple windows were proposed, see e.g., Messer (2019); Cho and Kirch (2020). They work in two steps: first change point candidates are generated for every single  $h$ , and afterwards all sets are merged giving final estimates. Despite improvements, the methods demand the selection of a window set that best accounts for the location of unknown change points.

The aim of this paper is to provide a MOSUM framework that overcomes window selection, but nevertheless exploits multiple windows to address change point occurrences on multiple time scales, denoted *multi-scale change point detection* algorithm (MSCP), see Algorithm 4.5. For that we extend the MOSUM perspective: instead of considering  $(D_{t,h})_t$  as a process of time  $t$  only, we let it depend on both  $t$  and  $h$ , i.e.,  $(D_{t,h})_{(t,h)}$ , while the indices  $(t, h)$  lie in a triangle  $\Delta_\delta \subset \mathbb{R}^2$ , see Figure 1 (top).  $\Delta_\delta$  is a right-angled and isosceles triangle, and the hypotenuse is oriented as the lower edge and refers to the smallest window  $h = \delta$  fixed. A higher horizontal slice refers to a larger  $h$ , and the upper vertex describes the largest  $h = \lfloor T/2 \rfloor$ .

The triangular structure follows from shrinkage of possible  $t$ -indices  $h, \dots, T - h$  when  $h$  increases. In Figure 1  $D_{t,h}$  is color-coded with  $D_{t,h} \approx 0$  green,  $> 0$  red, and  $< 0$  blue. At  $c_1 = 65$  there is an increase in  $\mu$  and thus  $D_{t,h} > 0$ , while at  $c_2 = 105$  and  $c_3 = 145$  a decrease in  $\mu$  yields  $D_{t,h} < 0$ , at least when  $h$  is not too large ( $h < 40$ ) such that only a single  $c_u$  is overlapped. The upper part of  $\Delta_\delta$  refers to larger  $h$  that result in an overlap of multiple change points. The area between  $c_1$  and  $c_2$  is green also for  $h$  large, at  $(t, h) \approx (85, 70)$ , because the parameters in the first and third section coincide and thus

the effects cancel out. In contrast, the area between  $c_2$  and  $c_3$  is dark blue for  $h$  large, at  $(t, h) \approx (120, 70)$ , as both changes at  $c_2$  and  $c_3$  are negative, which amplifies the effect and as a consequence simple argmax estimation would be flawed. Importantly, note that for smaller  $h$  large values of  $|D_{t,h}|$  concentrate around  $c_u \in C$ .

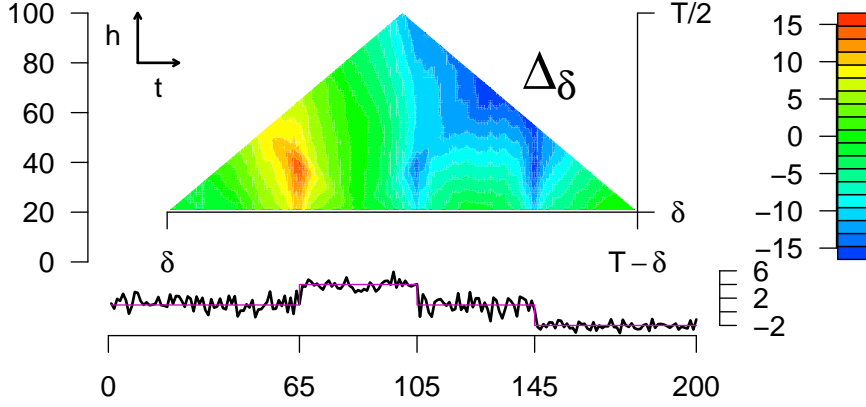


Figure 1: Bottom: Process via  $N(\mu, \sigma^2)$  RVs, with  $T = 200$ ,  $C = \{65, 105, 145\}$ ,  $\mu = 1, 4, 1, -2$  (pink),  $\sigma = 1, 0.8, 1, 0.5$ . Top:  $D_{t,h}$  with  $(t, h) \in \Delta_\delta$  for  $\delta = 20$ .

MSCP subsequently acts on subsets of  $\Delta_\delta$  by locally exploiting  $(D_{t,h})_{(t,h)}$ . The key ingredient is the construction of a *zigzag-path*, see Figure 2 (magenta): given a starting value  $(t_s, h_s)$  (pink circle), the path leads towards the lower edge of  $\Delta_\delta$  to some point  $(\hat{c}, \delta)$ , and  $\hat{c}$  functions as a change point estimate. The path evolves according to stepwise local argmax-estimation: in each instance the path moves one step downwards, i.e.,  $h$  switches to  $h - 1$  non-randomly. Then the path moves either one step left or right, or it stays, i.e.,  $t$  switches to some value in  $\{t - 1, t, t + 1\}$ , while the choice falls on the  $t$ -maximizer of  $|D_{t,h-1}|$ .

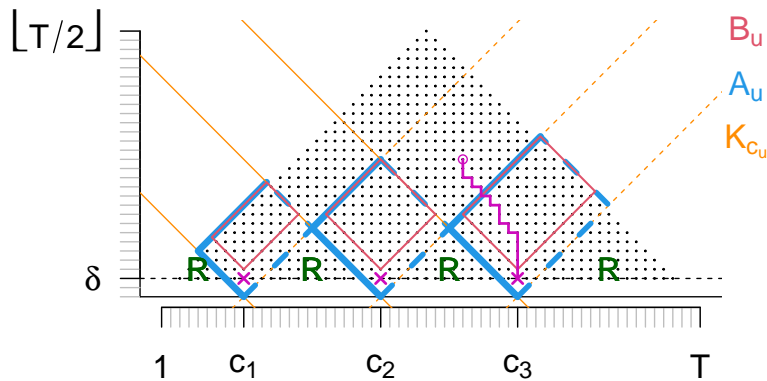


Figure 2: Representation of areas of attraction  $A_u$  (blue), inner sets  $B_u$  (red), cones  $K_{c_u}$  (orange) for three change points  $c_u$ , the remainder  $R$  (green), and a zigzag-path (magenta).

The idea of MSCP is the following, see also Figure 3: given a set  $S \subset \Delta_\delta$  of possible starting values (pink circles), the one maximizing  $h^{-1/2} \cdot |D_{t,h}|$  (i.e., the strongest 'signal to noise ratio') is the first starting point considered. Then its path delivers the first change point estimate  $\hat{c}$ . In order to avoid false positives, a breaking criterion is evaluated, which is computed from  $D_{t,h}$  on the path. If breaking is not demanded, then  $\hat{c}$  is accepted. In order to avoid multiple detections of the same change point, all elements of  $S$ , whose

paths could lead to  $\hat{c}$ , are deleted from  $S$  ('cut out cone'). Then estimation restarts, and iteratively change points are detected until the breaking criterion applies. In Figure 3 the algorithm estimates  $c_3$ ,  $c_1$  and  $c_2$ , and then the breaking criterion applies for the next candidate.

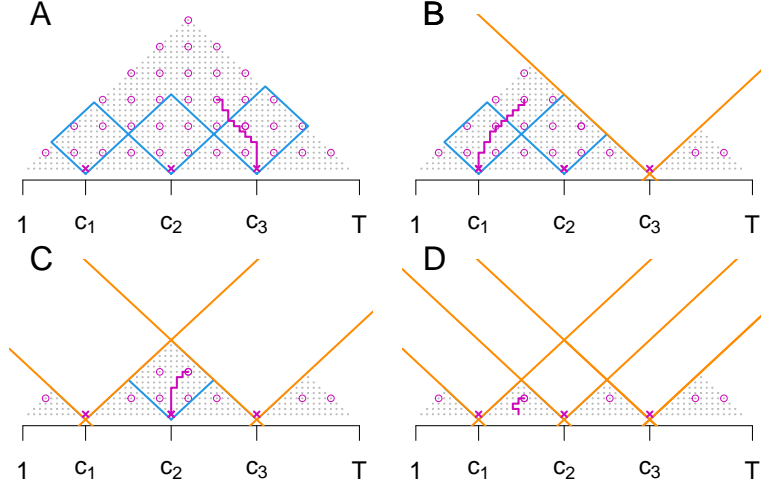


Figure 3: Schematic representation of MSCP. It is  $C = \{c_1, c_2, c_3\}$ . Subsequently  $c_3$ ,  $c_1$  and  $c_2$  are estimated, and then MSCP breaks .

The main result states strong consistency of MSCP for both the number and location of estimated change points. The crucial technical foundation relies on the path behavior: if the starting point  $(t_s, h_s)$  lies high enough on  $\Delta_\delta$ , i.e.,  $h_s$  large, then at some point the path enters a subset of  $\Delta_\delta$  that we call the *area of attraction*  $A_u$  of a change point  $c_u \in C$ , see Figure 2 (blue), and from this on it is systematically pushed towards the  $c_u$ .

For the process in Figure 4, MSCP yields estimates 145, 63 and 105, i.e., the number is correct, the smallest estimate at 63 is close to  $c_1 = 65$  and the other two estimates even hit the true  $c_2 = 105$  and  $c_3 = 145$ . MSCP is made available in the R-package `mscp` on CRAN (Levajkovic and Messer, 2021), which includes a summary and plotting routine. For the upper process given in Figure 1 it plots Figure 4, the top panel showing  $\Delta_\delta$  including  $S$  and the paths constructed, the middle panel giving the process and the means of the RVs in the detected sections (red), and the bottom showing the empirical variances therein (blue).

We strengthen three important upsides of MSCP: first, the method is non-parametric with weak distributional assumptions and thus allows to analyze a high variety of data. The consideration of additional changes in variance could be helpful in practice, as e.g., an increase in the mean might be accompanied with an increase in volatility. Second, the problem of window selection is overcome. Third, the gradual window adjustment improves the detection of change points on multiple time scales and different effects.

Estimation precision is supported in simulation studies by investigating different change point scenarios and effect sizes. Various distributions are considered, including normal, gamma, Poisson and binomial, and their combinations. Also, reasonable segmentation is shown for the evolution of COVID-19 cases in Zimbabwe in 2020.

The paper is organized as follows: In Section 2 we specify the model,  $\Delta_\delta$  and  $D_{t,h}$ . In Section 3 we study properties of  $(D_{t,h})_{(t,h) \in \Delta_\delta}$  which are used for change point detection.

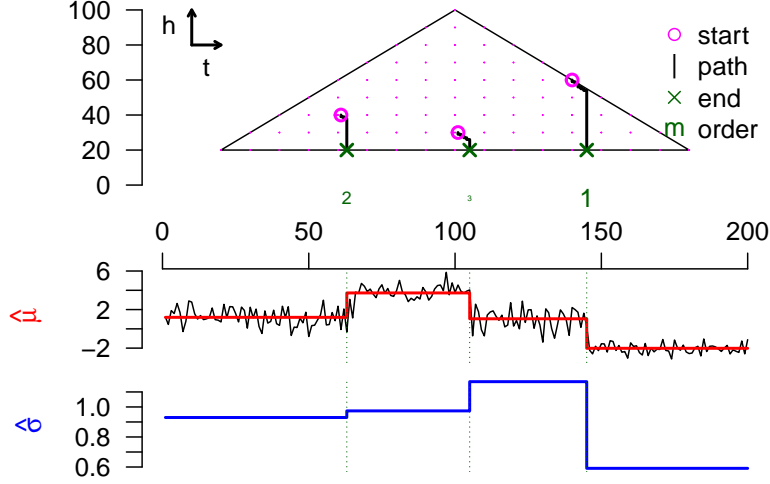


Figure 4: Plotting routine of the R-package `mscp`. It is  $\hat{C} = \{63, 105, 145\}$

In Section 4 we construct the zigzag-path and show that it yields proper estimates. We introduce the set of starting points  $S$ , define MSCP, and state consistency. In Section 5 we discuss the tuning parameters ( $\delta$ ,  $S$  and the breaking criterion), and present the simulations and the data example. Proofs are given in the Appendix 6.

## 2 The change point model and MOSUM on the triangle

**The model  $\mathcal{M}$**  We fix  $T \in \mathbb{N} \setminus \{0, 1\}$  and call  $\{1, \dots, T\}$  the observation regime. We consider a subset  $C \subset \{1, \dots, T-1\}$  of cardinality  $|C|$  with ordered elements  $c_1 < c_2 \dots < c_{|C|}$ . We call  $c_u$  the  $u$ -th change point and  $C$  the set of change points.  $C$  is treated fixed but unknown. Set  $c_0 := 0$  and  $c_{|C|+1} := T$ , and the minimal distance of adjacent change points  $\delta_C := \min_{u=1, \dots, |C|+1} (c_u - c_{u-1})$ .

Let  $(\Omega, \mathcal{A}, \mathbb{P})$  be a probability space and  $p > 0$ . We consider a triangular scheme: let  $(Z_{u,i})_{u,i}$  for  $u \in \{1, 2, \dots, |C| + 1\}$  and  $i = 1, 2, \dots$  be independent RVs in  $\mathcal{L}^{2+p}(\Omega, \mathcal{A}, \mathbb{P})$  with  $\mathbb{E}[Z_{u,i}] = 0$  and  $\text{Var}(Z_{u,i}) = 1$ , and let  $(Z_{u,i})_{i=1,2,\dots}$  be an i.i.d. sequence for each  $u$ . Further let  $\mu_1, \mu_2, \dots, \mu_{|C|+1} \in \mathbb{R}$  with  $\mu_u \neq \mu_{u+1}$ , and  $\sigma_1^2, \sigma_2^2, \dots, \sigma_{|C|+1}^2$  positive. For  $n \in \{1, 2, \dots\}$  set

$$X_i := \sum_{u=1}^{|C|+1} (\mu_u + \sigma_u Z_{u,i}) \cdot \mathbb{1}_{\{nc_{u-1}+1, \dots, nc_u\}}(i), \quad i \in \{1, 2, \dots, nT\}. \quad (2)$$

Dependence of  $X_i$  on  $n$  is suppressed for simplicity. The process  $\mathbf{X} := (X_i)_{i=1,2,\dots,nT}$  has  $|C|$  change points. In the section from  $nc_{u-1} + 1$  to  $nc_u$  it has expectation  $\mu_u$  and variance  $\sigma_u^2$ , which are then changing to  $\mu_{u+1}$  and  $\sigma_{u+1}^2$ . The case  $n = 1$  is considered the real-time scenario. Throughout, asymptotics are studied letting  $n \rightarrow \infty$ , i.e., the observation regime and all change points increase linearly. Given  $T$ , the set of processes  $\mathbf{X}$  constitutes the model  $\mathcal{M}$ .

For all  $u$ , we set the first two moments  $\mu_u^{(1)} := \mu_u$  and  $\mu_u^{(2)} := \sigma_u^2 + \mu_u^2$  and the centered moments  $\mu_u^{\{1\}} = 0$  and  $\mu_u^{\{2\}} := \sigma_u^2$ . If  $C = \emptyset$ , we set  $\mu := \mu^{(1)} := \mu_1^{(1)}$ ,  $\mu^{(2)} := \mu_1^{(2)}$  and  $\sigma^2 := \sigma_1^2 := \mu_1^{\{2\}}$ .

**The triangle  $\Delta_\delta$**  We define the index set  $\Delta_\delta$  of MOSUM. Fix a minimal window  $\delta \in \{1, 2, \dots, \lfloor T/2 \rfloor\}$ , where  $\lfloor \cdot \rfloor$  denotes the floor function. The window component is  $H_\delta := [\delta, T/2]$ , and for  $h \in H_\delta$  the time slice is  $T_h := [h, T - h]$ . Then we set  $\Delta_\delta := \{(t, h) \mid t \in T_h, h \in H_\delta\}$ .

**Local estimators and MOSUM** For  $(t, h) \in \Delta_\delta$  we consider indices interpreted a left and right window  $I_\ell^{(n)} := \{\lfloor nt \rfloor - \lfloor nh \rfloor + 1, \dots, \lfloor nt \rfloor\}$  and  $I_r^{(n)} := \{\lfloor nt \rfloor + 1, \dots, \lfloor nt \rfloor + \lfloor nh \rfloor\}$ . We set local estimators for  $\mu^{(k)}$  and  $\mu^{\{k\}}$  for  $j \in \{\ell, r\}$  via

$$\hat{\mu}_j^{(k)} := \frac{1}{nh} \sum_{i \in I_j^{(n)}} X_i^k \quad \text{and} \quad \hat{\mu}_j^{\{k\}} := \frac{1}{nh} \sum_{i \in I_j^{(n)}} (X_i - \hat{\mu}_j^{(1)})^k, \quad (3)$$

and abbreviate  $\hat{\mu}_j := \hat{\mu}_j^{(1)}$  and  $\hat{\sigma}_j^2 := \hat{\mu}_j^{\{2\}}$ . Dependence on  $t$  and  $h$  is suppressed to avoid overload. Then we define

$$D_{t,h}^{(n)} := \frac{\hat{\mu}_r - \hat{\mu}_\ell}{[(\hat{\sigma}_r^2 + \hat{\sigma}_\ell^2)/\lfloor nh \rfloor]^{1/2}}, \quad (4)$$

noting that  $D_{t,h}^{(1)} = D_{t,h}$  from (1). We set  $D_{t,h}^{(n)} := 0$  if the denominator vanishes. For each  $n$  the statistics are càdlàg step-functions in both directions  $t$  and  $h$ , with discontinuities in horizontal and vertical slices at values  $k/n$ , see Figure 5.

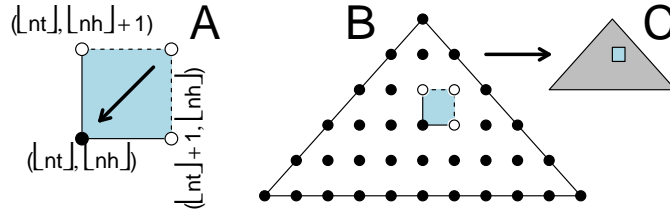


Figure 5: Process construction. The floor-functions (A) in  $I_j^{(n)}$ ,  $j \in \{\ell, r\}$  for both  $\lfloor nt \rfloor$  and  $\lfloor nh \rfloor$  appear within a factor- $n$ -enlarged triangle (B), which is rescaled to  $\Delta_\delta$  (C).

Processes are considered in function space  $(\mathcal{D}_{\mathbb{R}}[\mathcal{K}], \|\cdot\|_\infty)$ . For a convex subset  $\mathcal{K}$  of  $\mathbb{R}^k$  with  $k \in \{1, 2\}$  let  $\mathcal{D}_{\mathbb{R}}[\mathcal{K}]$  denote the set of  $\mathbb{R}$ -valued functions on  $\mathcal{K}$ , which in case of  $k = 1$  are càdlàg, and in case of  $k = 2$  càdlàg with respect to each component when the other component is fixed.  $\mathcal{D}_{\mathbb{R}}[\mathcal{K}]$  is endowed with uniform distance  $\|\cdot\|_\infty$ . As asymptotics yield almost surely (a.s.) continuous limits, there is no need to evoke Skorokhod topology.

### 3 Asymptotics of the estimators

**Strong consistency** We state strong convergence of the estimators. We define their limits pointwise for  $(t, h) \in \Delta_\delta$ . They are weightings of the theoretical moments depending on the change point locations relative to the window. Consider the left window  $(t - h, t]$  and assume that the change points that are overlapped are  $C_\ell \subset C$ , i.e., we find  $t - h < c_{\ell,1} < c_{\ell,2} < \dots < c_{\ell,|C_\ell|} \leq t$ , and  $c_{\ell,u}$  denotes the  $u$ -th smallest change point in  $C_\ell$ . Set  $c_{\ell,0} := t - h$  and  $c_{\ell,|C_\ell|+1} := t$ . For  $u = 1, 2, \dots, |C_\ell| + 1$  set the distance  $d_{\ell,u} := c_{\ell,u} - c_{\ell,u-1}$  between adjacent change points. The moments related to these sections are abbreviated by  $\mu_{\ell,u}^{(k)}$  and  $\sigma_{\ell,u}^2$ , see Figure 6 left. From this we set

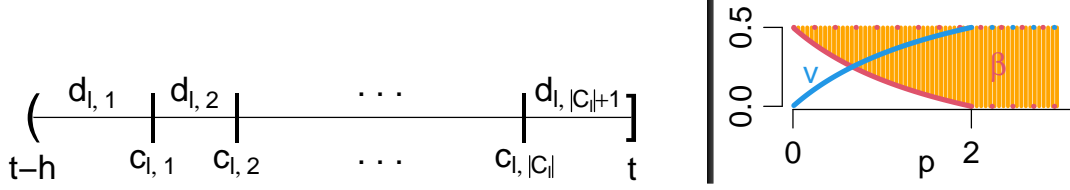


Figure 6: Left: schematic representation of the left window overlapping  $|C_\ell|$  change points. Right: Parameters  $v$  and  $\beta$  depending on  $p$ .

$$\tilde{\mu}_\ell^{(k)} := \sum_{u=1}^{|C_\ell|+1} \frac{d_{\ell,u}}{h} \cdot \mu_{\ell,u}^{(k)} \quad \text{and} \quad \tilde{\sigma}_\ell^2 := \sum_{u=1}^{|C_\ell|+1} \frac{d_{\ell,u}}{h} \cdot [\sigma_{\ell,u}^2 + (\tilde{\mu}_\ell - \mu_{\ell,u})^2], \quad (5)$$

with  $\tilde{\mu}_\ell := \tilde{\mu}_\ell^{(1)}$ . The limits weight the moments with the time  $d_{\ell,u}$  spent in a section relative to the window length  $h = \sum_u d_{\ell,u}$ . Further we set

$$\tilde{\tilde{\sigma}}_\ell^2 := \sum_{u=1}^{|C_\ell|+1} \frac{d_{\ell,u}}{h} \cdot \sigma_{\ell,u}^2, \quad \text{and} \quad e_\ell^2 := \sum_{u=1}^{|C_\ell|+1} \frac{d_{\ell,u}}{h} (\tilde{\mu}_\ell - \mu_{\ell,u})^2, \quad (6)$$

and note that  $\tilde{\sigma}_\ell^2 = \tilde{\tilde{\sigma}}_\ell^2 + e_\ell^2$ , i.e.,  $\tilde{\sigma}_\ell^2$  weights not only the variances  $\sigma_{\ell,u}^2$  as in  $\tilde{\tilde{\sigma}}_\ell^2$ , but also the additional error term  $e_\ell^2$ . The error accounts for the violation of change points in the calculation of the mean in the computation of the empirical variance – the mean is calculated from all data in the windows 'violating' unknown change points. It is  $e_\ell^2 \geq 0$ . If no change points are overlapped  $C_\ell = \emptyset$ , then the limits simplify to single theoretical moments  $\tilde{\mu}_\ell^{(k)} = \mu_{\ell,1}^{(k)}$  and  $\tilde{\tilde{\sigma}}_\ell^2 = \tilde{\sigma}_\ell^2 = \sigma_{\ell,1}^2$  and also  $e_\ell^2 = 0$ . Analogously we define the limits  $\tilde{\mu}_r^{(k)}$  and  $\tilde{\sigma}_r^2$  for the right window  $(t, t+h]$  by considering the change points  $C_r$  whose ordered elements  $c_{r,u}$  fulfill  $t < c_{r,1} < c_{r,2} < \dots < c_{r,|C_r|} \leq t+h$ . If  $C = \emptyset$ , then for all  $(t, h) \in \Delta_\delta$  we obtain the population parameters  $\tilde{\mu}_j = \mu$ ,  $\tilde{\sigma}_j^2 = \sigma^2$  etc. In the following we state strong consistency of the estimators.

**Lemma 3.1.** *Let  $\mathbf{X} \in \mathcal{M}$ . For  $j \in \{\ell, r\}$  it holds in  $(\mathcal{D}_\mathbb{R}[\Delta_\delta], \|\cdot\|_\infty)$  a.s. as  $n \rightarrow \infty$*

$$n^v \cdot (\hat{\mu}_j^{(k)} - \tilde{\mu}_j^{(k)})_{(t,h)} \longrightarrow (0)_{(t,h)} \quad \text{for } v \in \begin{cases} (-\infty, 1/2), & \text{if } k = 1, \\ (-\infty, 1/2) \cap (-\infty, p/(p+2)], & \text{if } k = 2, \end{cases}$$

and  $n^v \cdot (\hat{\sigma}_j^2 - \tilde{\sigma}_j^2)_{(t,h)} \rightarrow (0)_{(t,h)}$  with  $v \in (-\infty, 1/2) \cap (-\infty, p/(p+2)]$ .

The result follows from the Marcinkiewicz-Zygmund SLLN, noting that  $\mathbb{E}[|X_i|^{2+p}] < \infty$ . See  $v$  in Figure 6 right: for  $k = 1$  we cannot reach  $1/2$  noting CLT and LIL, and for  $k = 2$  the rate improves with the existence of higher moments via  $p$ , but only for  $p < 2$  while  $p/(2+p) < 1/2$ , i.e.,  $p \geq 2$  brings no improvement. Any rate for  $k = 2$  is valid for  $k = 1$ .

The systematic component of  $(D_{t,h}^{(n)})_{(t,h) \in \Delta_\delta}$  is the centering  $(d_{t,h}^{(n)})_{(t,h) \in \Delta_\delta}$  given by

$$d_{t,h}^{(n)} := \frac{\tilde{\mu}_r - \tilde{\mu}_\ell}{[(\tilde{\sigma}_r^2 + \tilde{\sigma}_\ell^2)/[nh]]^{1/2}}. \quad (7)$$

We note that  $n^{-1/2} \cdot d_{t,h}^{(n)} = d_{t,h}^{(1)}$  and conclude from Lemma 3.1

**Corollary 3.2.** *Let  $\mathbf{X} \in \mathcal{M}$ . For  $v \in (-\infty, 1/2) \cap (-\infty, p/(p+2)]$  it holds in  $(\mathcal{D}_{\mathbb{R}}[\Delta_\delta], \|\cdot\|_\infty)$  a.s. as  $n \rightarrow \infty$*

$$n^v \cdot \left( \frac{1}{\sqrt{n}} D_{t,h}^{(n)} - d_{t,h}^{(1)} \right)_{(t,h)} \rightarrow (0)_{(t,h)}.$$

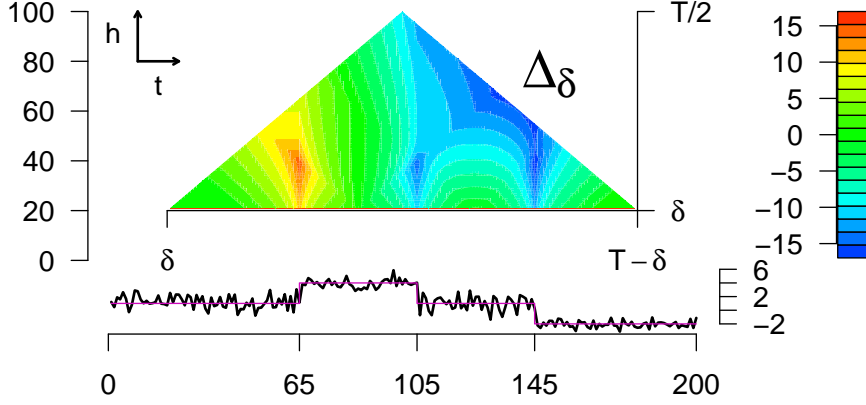


Figure 7:  $d_{t,h}^{(1)}$  relating to  $D_{t,h}^{(1)}$  from Figure 1.

Figure 7 shows  $d_{t,h}^{(1)}$  relating to  $D_{t,h}^{(1)}$ . It has an analogous shape, but smoother as noise is canceled out. We will construct the zigzag-path from  $D_{t,h}^{(n)}$  and deduce properties from a non-random path based on  $d_{t,h}^{(n)}$ .

**Considering a single change point** We describe  $(d_{t,h}^{(n)})_t$  for fixed  $h$  as a function of  $t$ . Let  $c_u \in C$ . We assume  $h$  small such that only  $c_u$  is overlapped by the double-window when it is near  $c_u$ . We formalize the shape of  $(d_{t,h}^{(n)})_t$  in Lemma 3.3, which will be used to show that the zigzag-path is pushed towards  $c_u$  when it comes close to it.

If  $c_{u+1} - c_u \geq h$  and  $c_u - c_{u-1} > h$ , then set  $\tau_h := [c_{u-1} + h, c_{u+1} - h)$ , else set  $\tau_h := \emptyset$ . For  $h$  small it is  $\tau_h \neq \emptyset$ . In this case  $(d_{t,h}^{(n)})_{t \in \tau_h}$  is continuous, it vanishes if  $|t - c_u| \geq h$  because no  $c \in C$  is overlapped, and it systematically deviates from zero if  $|t - c_u| < h$  with extreme value  $t = c_u$ , see Figure 8E in which the blue and red lines indicate a uniform bound for the derivative. We set  $v_{t,h} := [(\tilde{\sigma}_r^2 + \tilde{\sigma}_\ell^2) / (\tilde{\sigma}_r^2 + \tilde{\sigma}_\ell^2)]^{1/2}$ , recalling  $\tilde{\sigma}_j^2 = \tilde{\sigma}_j^2 + e_j^2$ , see (5) and (6), and denote  $\wedge$  the minimum and  $\vee$  the maximum.

**Lemma 3.3.** *Let  $\mathbf{X} \in \mathcal{M}$ ,  $c_u \in C$  and  $h$  be fixed such that  $\tau_h \neq \emptyset$ . Then both  $(d_{t,h}^{(n)})_{t \in \tau_h}$  and  $(v_{t,h} \cdot d_{t,h}^{(n)})_{t \in \tau_h}$  are continuous and zero for  $t \in \tau_h \setminus [c_u - h, c_u + h)$ . For  $t \in [c_u - h, c_u + h)$ , four cases are differentiated regarding  $d_{t,h}^{(n)}$ : for  $\mu_{u+1} > \mu_u$  we find that*

$$d_{t,h}^{(n)} \text{ is } \begin{cases} \text{strictly increasing for } t \in [c_u - h, c_u], \\ \text{strictly decreasing for } t \in (c_u, c_u + h]. \end{cases} \quad (8)$$

For  $\mu_{u+1} < \mu_u$  it is 'increasing' and 'decreasing' replaced. Further, for  $t \in (c_u - h, c_u) \cup (c_u, c_u + h)$  it is

$$\sqrt{nh} \cdot \kappa_a \leq \left| \frac{\partial}{\partial t} d_{t,h}^{(n)} \right| \leq \sqrt{nh} \cdot \kappa_b, \quad (9)$$



with constants

$$\kappa_a := |\mu_{u+1} - \mu_u| \cdot \frac{2(\sigma_{u+1}^2 \wedge \sigma_u^2)}{[2(\sigma_{u+1}^2 \vee \sigma_u^2) + (\mu_{u+1} - \mu_u)^2/4]^{3/2}},$$

$$\kappa_b := |\mu_{u+1} - \mu_u| \cdot \frac{2(\sigma_{u+1}^2 \vee \sigma_u^2) + (\mu_{u+1} - \mu_u)^2}{[2(\sigma_{u+1}^2 \wedge \sigma_u^2)]^{3/2}}.$$

Regarding  $v_{t,h} \cdot d_{t,h}^{(n)}$  six cases are differentiated: for  $\mu_{u+1} > \mu_u$  and

$$\sigma_{u+1}^2 = \sigma_u^2 : v_{t,h} \cdot d_{t,h}^{(n)} \text{ is } \begin{cases} \text{linear and strictly increasing for } t \in [c_u - h, c_u], \\ \text{linear and strictly decreasing for } t \in (c_u, c_u + h]. \end{cases}$$

$$\sigma_{u+1}^2 > \sigma_u^2 : v_{t,h} \cdot d_{t,h}^{(n)} \text{ is } \begin{cases} \text{strictly concave and strictly increasing for } t \in [c_u - h, c_u], \\ \text{strictly convex and strictly decreasing for } t \in (c_u, c_u + h]. \end{cases}$$

$$\sigma_{u+1}^2 < \sigma_u^2 : v_{t,h} \cdot d_{t,h}^{(n)} \text{ is } \begin{cases} \text{strictly convex and strictly increasing for } t \in [c_u - h, c_u], \\ \text{strictly concave and strictly decreasing for } t \in (c_u, c_u + h]. \end{cases}$$

For  $\mu_{u+1} < \mu_u$ , the expressions hold true, but with 'convex' and 'concave' as well as 'increasing' and 'decreasing' replaced. It is  $v_{t,h} \cdot |d_{t,h}^{(n)}| \geq |d_{t,h}^{(n)}|$  with equality at  $t = c_u$ .

Both  $(v_{t,h} \cdot d_{t,h}^{(n)})_t$  and  $(d_{t,h}^{(n)})_t$  are depicted in Figure 8D and E.

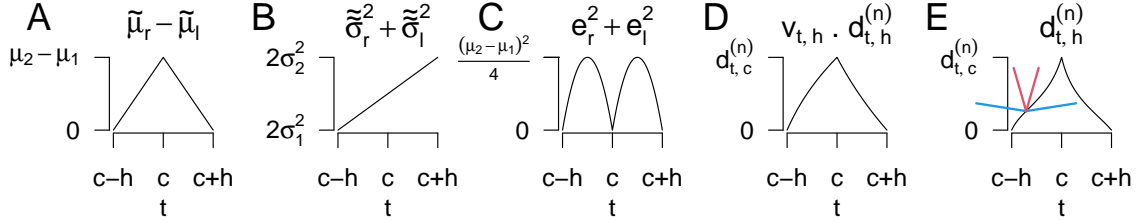


Figure 8: Construction of  $(d_{t,h}^{(n)})_{t \in \tau_h}$  (for  $c = c_1$ ). A:  $\tilde{\mu}_r - \tilde{\mu}_\ell$ , B:  $\tilde{\sigma}_r^2 + \tilde{\sigma}_\ell^2$ , C:  $e_r^2 + e_\ell^2$ , D:  $v_{t,h} \cdot d_{t,h}^{(n)}$ , E:  $d_{t,h}^{(n)}$  and lines with slopes  $\mp(nh)^{1/2} \cdot \kappa_a$  (blue) and  $\mp(nh)^{1/2} \cdot \kappa_b$  (red).

Figure 8 shows the statistics that factor into  $(d_{t,h}^{(n)})_{t \in \tau_h}$ . It is  $\mu_2 > \mu_1$  and  $\sigma_2^2 > \mu_2^2$ . The function  $\tilde{\mu}_r - \tilde{\mu}_\ell$  has the shape of a hat (A). It is positive as  $\mu_2 > \mu_1$ . The function  $\tilde{\sigma}_r^2 + \tilde{\sigma}_\ell^2$  is linear (B). It is increasing as  $\sigma_2^2 > \sigma_1^2$ . The error  $e_r^2 + e_\ell^2$  describes two parabolas and vanishes outside the  $h$ -neighborhood of  $c := c_u$  and also at  $c$  (C). The error is maximal at  $c \mp h/2$  which are the points where either the right or the left window is divided in half and thus equally sharing the left and right population. Panel D shows  $v_{t,h} \cdot d_{t,h}^{(n)}$  which is  $(nh)^{1/2}$  times (A) divided by the square-root of (B). It is non-negative as  $\mu_2 > \mu_1$  and concave on  $[c - h, c]$  and convex on  $(c, c + h]$  as  $\sigma_2^2 > \sigma_1^2$ . Panel D shows  $d_{t,h}^{(n)}$  which is  $(nh)^{1/2}$  times (A) divided by the square-root of the sum of (B) and (C). As  $\mu_2 > \mu_1$ , it is strictly increasing in  $[c - h, c]$  and strictly decreasing on  $(c, c + h]$ . It is  $v_{t,h} \cdot d_{t,h}^{(n)} \geq d_{t,h}^{(n)}$ , as  $v_{t,h} \geq 1$ . Note that in Lemma 3.3 it is  $0 < \kappa_a < \kappa_b < \infty$ , and  $\kappa_a, \kappa_b$  depend only on the population parameters, such that the bounds for the derivative in (9) depend on  $h$  but not on  $t$ . The upper bound  $(nh)^{1/2} \cdot \kappa_b$  is a Lipschitz constant for  $(d_{t,h}^{(n)})_t$ . Figure 8E shows lines with slopes  $\mp(nh)^{1/2} \cdot \kappa_a$  (blue) and  $\mp(nh)^{1/2} \cdot \kappa_b$  (red), i.e., the slope of  $(d_{t,h}^{(n)})_t$  varies in between for all  $t \in (c_u - h, c_u) \cup (c_u, c_u + h)$ .

**Weak convergence** We state weak convergence of  $(D_{t,h}^{(n)})_{(t,h) \in \Delta_\delta}$  if  $C = \emptyset$ . Let  $(W_t)_{t \geq 0}$  be a standard Brownian motion. Then define  $(L_{t,h})_{(t,h) \in \Delta_\delta}$  via  $L_{t,h} := (2h)^{-1/2} \cdot [(W_{t+h} - W_t) - (W_t - W_{t-h})]$ . The process  $(L_{t,h})_{(t,h)}$  is continuous with  $L_{t,h} \sim N(0, 1)$ .

**Proposition 3.4.** *Let  $\mathbf{X} \in \mathcal{M}$  with  $C = \emptyset$ . In  $(\mathcal{D}_{\mathbb{R}}[\Delta_\delta], \|\cdot\|_\infty)$  it holds as  $n \rightarrow \infty$  that  $(D_{t,h}^{(n)})_{(t,h)} \xrightarrow{d} (L_{t,h})_{(t,h)}$ .*

$L_{t,h}$  preserves the double-window structure of  $D_{t,h}^{(n)}$ , zero mean aligns with  $C = \emptyset$  and unit variance results from scaling of  $D_{t,h}^{(n)}$ . The proof applies Donsker's theorem.

## 4 Change point detection via MSCP

**Segmentation of the triangle** We specify regions of  $\Delta_\delta$ . Each  $c_u \in C$  has an area of attraction  $A_u := \{(t, h) \in \Delta_\delta : c_{u-1} \leq t - h < c_u \leq t + h < c_{u+1}\}$ , see Figure 2 (blue). For all  $(t, h) \in A_u$  the associated double window overlaps  $c_u$  but no other change point. It is  $|d_{t,h}^{(n)}| > 0$  for  $(t, h) \in A_u$ . We show that path that starts in  $A_u$  is systematically pushed towards  $c_u$ , such that its endpoint becomes a proper estimate for  $c_u$ . We also set  $B_u := \{(t, h) \in A_u : |t - c_u| \leq h - \delta + 1\}$ , for whose elements we find the 't-distance' to  $c_u$  smaller than the 'h-distance' (plus 1) to the bottom of  $\Delta_\delta$ . For any  $t_0 \in [\delta, T - \delta]$  we define its cone  $K_{t_0} := \{(t, h) \in \Delta_\delta : t - h < t_0 \leq t + h\}$ . The cones  $K_{c_u}$  of the  $c_u \in C$  are shown in Figure 2 (orange).  $K_{c_u}$  consists of all  $(t, h) \in \Delta_\delta$  for which the double window overlaps  $c_u$  and possibly neighboring change points. It holds  $B_u \subset A_u \subset K_{c_u} \subset \Delta_\delta$ . Finally, we consider the remainder  $R := \Delta_\delta \setminus \bigcup_{u=1}^{|C|} K_{c_u}$ , that consists of  $(t, h) \in \Delta_\delta$  for which no  $c_u$  is overlapped by the double window, such that  $d_{t,h}^{(n)} = 0$  for all  $(t, h) \in R$ . In Figure 2,  $R$  consists of four subtriangles of  $\Delta_\delta$  as there are three change points involved.

**The zigzag-downpath** We construct a path on  $\Delta_\delta \cap \mathbb{N}^2$  w.r.t. either  $D_{t,h}^{(n)}$  or  $d_{t,h}^{(n)}$ .

**Algorithm 4.1.** (*zigzag-downpath*)

*Input:*  $\mathbf{X} \in \mathcal{M}$  and a starting value  $(t_s, h_s) \in \Delta_\delta \cap \mathbb{N}^2$ . Set  $f_{t,h}^{(n)} \in \{d_{t,h}^{(n)}, D_{t,h}^{(n)}\}$ .

*Construction:* set  $t_s^{(n)}(0) := \min \left( \operatorname{argmax}_{t \in \{t_s-1, t_s, t_s+1\} \cap \Delta_\delta} n^{-1/2} \cdot |f_{t,h_s}^{(n)}| \right)$ . For  $k = 1, 2, \dots, h_s - \delta$  iteratively define

$$t_s^{(n)}(k) := \min \left( \operatorname{argmax}_{t \in \{t_s^{(n)}(k-1)-1, t_s^{(n)}(k-1), t_s^{(n)}(k-1)+1\}} n^{-1/2} \cdot |f_{t, h_s-k}^{(n)}| \right). \quad (10)$$

*Output:* the zigzag downpath  $(t_s^{(n)}(k), h_s - k)_{k=0,1,2,\dots,h_s-\delta}$ .

In  $t_s^{(n)}(0)$  we start with choosing the maximizer among  $\{t_s - 1, t_s, t + 1\} \cap \Delta_\delta$  and the restriction to  $\Delta_\delta$  yields well-definedness if  $(t_s, h_s)$  lies on its edge. The minimum in  $t_s^{(n)}(k)$  ensures uniqueness. For  $f_{t,h}^{(n)} = D_{t,h}^{(n)}$  the maximum is necessarily a.s. unique in case the RVs of  $\mathbf{X}$  lack point masses. We abbreviate the end  $t_e^{(n)} := t_s^{(n)}(h_s - \delta)$ . In order to differentiate the paths we write

$$t_s^{(n)}(k) =: \begin{cases} t_s(k), & \text{if } f_{t,h}^{(n)} = d_{t,h}^{(n)}, \\ \hat{t}_s^{(n)}(k), & \text{if } f_{t,h}^{(n)} = D_{t,h}^{(n)}, \end{cases} \quad (11)$$

and accordingly  $t_e$  and  $\hat{t}_e^{(n)}$ , noting that for  $f_{t,h}^{(n)} = d_{t,h}^{(n)}$  the path is independent of  $n$ , as  $n^{-1/2} \cdot |d_{t,h}^{(n)}| = |d_{t,h}^{(1)}|$ .

**Path behavior w.r.t  $d_{t,h}^{(n)}$**  A path starting in  $A_u$  systematically tends towards  $c_u$ :

**Lemma 4.2.** *Let  $\mathbf{X} \in \mathcal{M}$ ,  $c_u \in C$  and  $f_{t,h}^{(n)} = d_{t,h}^{(n)}$ . If  $(t_s, h_s) \in A_u$ , then for all  $k \in \{1, 2, \dots, h_s - \delta\}$  it holds*

$$t_s(k) - t_s(k-1) = \begin{cases} 0, & \text{if } |t_s - c_u| \leq k, \\ 1, & \text{if } t_s < c_u - k, \\ -1, & \text{if } t_s > c_u + k, \end{cases} \quad (12)$$

If  $(t_s, h_s) \in B_u$ , then  $t_e = c_u$ . If  $(t_s, h_s) \in A_u \setminus B_u$ , then  $|t_e - c_u| \leq \delta - 1$ .

Lemma 4.2 states that in each step  $t_s(k)$  either increases by unity if  $t_s < c_u$  or it decreases by unity if  $t_s > c_u$ , and if it reaches  $c_u$  then it stays. Thus, the path  $(t_s(k), h_s - k)_k$  is perfectly zigzagging towards the vertical line at  $c_u$ . If it reaches this line then it moves vertically downwards to the lower edge of  $\Delta_\delta$ , i.e.,  $t_e = c_u$ . The proof exploits the shape of  $(d_{t,h}^{(n)})_t$  stated in Lemma 3.3.

**Path behavior w.r.t  $D_{t,h}^{(n)}$**  Regarding  $D_{t,h}^{(n)}$ , a path starting in  $A_u$  converges towards the path w.r.t.  $d_{t,h}^{(n)}$ :

**Proposition 4.3.** *Let  $\mathbf{X} \in \mathcal{M}$ ,  $c_u \in C$  and  $f_{t,h}^{(n)} = D_{t,h}^{(n)}$ . Let  $(t_s, h_s) \in A_u$ , then for all  $k \in \{0, 1, 2, \dots, h_s - \delta\}$  it holds that  $\hat{t}_s^{(n)}(k) \rightarrow t_s(k)$  a.s. as  $n \rightarrow \infty$  for all  $k$ , while  $t_s(k)$  is given in (12).*

Consequently, starting in  $A_u$  yields detection of  $c_u$  up to a distance of  $\delta - 1$ . More precisely, for  $(t_s, h_s) \in B_u$  we find  $\lim_{n \rightarrow \infty} \hat{t}_e^{(n)} = c_u$  a.s., and for  $(t_s, h_s) \in A_u \setminus B_u$  it is  $\lim_{n \rightarrow \infty} |\hat{t}_e^{(n)} - c_u| \leq \delta - 1$  a.s. The proof exploits closeness of  $D_{t,h}^{(n)}$  and  $d_{t,h}^{(n)}$ .

**Starting points** We call a set  $S \subset \mathbb{N}^2 \cap \Delta_\delta$  a sufficient set of starting points if  $S \cap A_u \neq \emptyset$  for all  $u = 1, \dots, |C|$ , i.e., for all  $c_u \in C$  there lies a starting point in  $A_u$ . For a mesh size  $g \in \mathbb{N}$  set a grid  $S_g := (g \cdot \mathbb{N}^2) \cap \Delta_\delta$ , see Figure 3A (pink dots).

**Lemma 4.4.** *Let  $\mathbf{X} \in \mathcal{M}$  and  $[\delta] < [\delta_C/2]$ . A grid  $S_g$  is sufficient if  $g \leq \lfloor \delta_C/2 \rfloor$ .*

The proof applies geometry. When a path enters  $A_u$ , then  $c_u$  is detected up to a distance of  $\delta - 1$ , see Proposition 4.3. Thus, when considering all paths starting in  $S$ , then all  $c \in C$  will be detected. We need to avoid multiple detections of any  $c$  as well as false positives.

**Change point detection** Set  $\min \emptyset := \infty$ , and for a set  $F$  denote  $U(F)$  a uniformly sampled element.

**Algorithm 4.5.** (MSCP)

*Input:*  $\mathbf{X} \in \mathcal{M}$ , a set of starting values  $S$ ,

and constants  $\kappa > 0$ , and  $\beta \in [1/2 - v, 1/2)$  for  $v \in (0, 1/2) \cap (0, p/(p+2)]$ .

Initialize: counter  $m = 1$ , estimates  $\hat{C}_m^{(n)} = \emptyset$  and starting values  $S_m^{(n)} = S$ .

While  $S \neq \emptyset$ , loop:

1. Choose the starting value  $(\hat{t}_{s,m}^{(n)}, \hat{h}_{s,m}^{(n)}) := U(\operatorname{argmax}_{(t,h) \in S_m^{(n)}} [(nh)^{-1/2} \cdot |D_{t,h}^{(n)}|])$ .
2. Run the zigzag-path w.r.t.  $(\hat{t}_{s,m}^{(n)}, \hat{h}_{s,m}^{(n)})$  and  $f_{t,h}^{(n)} = D_{t,h}^{(n)}$ ,  
call the path  $(\hat{t}_{s,m}^{(n)}(k), \hat{h}_{s,m}^{(n)} - k)_{k=0,1,2,\dots,\hat{h}_{s,m}^{(n)}-\delta}$  and the endpoint  $(\hat{t}_{e,m}^{(n)}, \delta)$ ,  
and compute the minimal distance  $\mathcal{D}_m^{(n)} := \min\{|\hat{t}_{e,m}^{(n)} - \hat{c}^{(n)}| : \hat{c}^{(n)} \in \hat{C}^{(n)}\}$ .
3. Check for multiple detections (3a.) and false positives (3b.)
  - 3a. If  $\mathcal{D}_m^{(n)} \leq 2(\delta - 1)$ , then set  $S_m^{(n)} := S_m^{(n)} \setminus K_{\hat{t}_{e,m}^{(n)}}$  and Goto 1.
  - 3b. If  $\max_{k=0,1,\dots,\hat{h}_{s,m}^{(n)}-\delta} |D_{\hat{t}_{s,m}^{(n)}(k), \hat{h}_{s,m}^{(n)}-k}^{(n)}| < \kappa \cdot n^\beta$ , then break the loop.
  - [3c. Optional: If  $\mathcal{D}_m^{(n)} < \delta_C - 2(\delta - 1)$ , then break the loop. (Needs input  $\delta_C$ .)]
4. Update  $m = m + 1$ , then set  $\hat{C}_m^{(n)} = \hat{C}_{m-1}^{(n)} \cup \{\hat{t}_{e,m-1}^{(n)}\}$  and  $S_m^{(n)} = S_{m-1}^{(n)} \setminus K_{\hat{t}_{e,m-1}^{(n)}}$ ,  
and Goto 1.

Output:  $\hat{C}^{(n)} := \hat{C}_m^{(n)}$ .

The parameters  $\kappa$  and  $\beta$  yield a threshold  $\kappa \cdot n^\beta$  (in 3b.), and if chosen large then this supports breaking the algorithm. Recall  $E[|X_1|^{2+p}] < \infty$ .  $\beta$  is related to  $p$  via  $v$ , see Figure 6 right. Small  $p$  forces  $\beta$  close to  $1/2$  and a larger  $p$  allows for smaller  $\beta$ . The parameter  $\beta$  is redundant if  $n = 1$ . In 1., the maximum is a.s. unique if the RVs of  $\mathbf{X}$  do not have point masses. In general, uniform sampling yields well-definedness. It is  $\mathcal{D}_1^{(n)} = \infty$ .

Algorithm 4.5 (MSCP) is depicted in Figure 3. Successively,  $C$  is estimated. We comment on the steps.

- 1.: Among all current starting points the one maximizing  $(nh)^{-1/2} \cdot |D_{t,h}^{(n)}|$  is chosen, uniformly in case of non-uniqueness.
- 2.: The zigzag-path is constructed and  $\hat{t}_{e,m}^{(n)}$  functions as a change point candidate. The minimal distance  $\mathcal{D}_m^{(n)}$  of  $\hat{t}_{e,m}^{(n)}$  and all previous estimates is computed.
- 3.: Two aspects are addressed:
  - 3a.: 'Avoiding multiple detections': if  $\mathcal{D}_m^{(n)} \leq 2(\delta - 1)$ , then  $\hat{t}_{e,m}^{(n)}$  is rejected, all starting points from its cone are cut, and estimation restarts. The rationale is that if the paths of both  $\hat{t}_{e,m}^{(n)}$  and the closest estimate passed  $A_u$ , then they also systematically led to  $c_u$  up to  $\delta - 1$ . Hence, rejection of such  $\hat{t}_{e,m}^{(n)}$  avoids multiple detections.
  - 3b.: 'Avoiding false positives': if  $\hat{t}_{e,m}^{(n)}$  was not rejected in 3a., then decision is made of whether the loop breaks. If the objection function takes extreme values on the zigzag-path, then this supports  $\hat{t}_{e,m}^{(n)}$  to indicate an  $c_u \in C$ , and thus it is accepted in 4., and the next iteration starts after the cone of  $\hat{t}_{e,m}^{(n)}$  is cut to avoid further detections of  $c_u$ .

Note that we allow an error up to  $\delta - 1$ , and if the distance of  $\hat{t}_{e,m}^{(n)}$  to  $c_u$  is positive, then a slightly shifted cone was cut. This gives rise for 3a. at first. Also note that if all  $c \in C$  are detected and near cones are cut (again mentioning 3a.), then what is eventually

left over is the remainder  $R$ . Thus, on the next path the objection function will no longer take extreme values which support breaking in 3b., and the previous estimates are returned. Finally note that the breaking criterion 3c. applies if the minimal distance between change points was exceeded, also accounting for estimation precision only up to  $\delta - 1$ . Asymptotically, this will not occur, so 3c. is obsolete for theoretical consistency, but may be used in practice.

We denote  $\hat{c}_u^{(n)}$  the  $u$ -th smallest element of  $\hat{C}^{(n)}$ . For well-definedness, if  $|\hat{C}^{(n)}| < |C|$  set  $\hat{c}_u^{(n)} := 0$  for all  $u = |\hat{C}^{(n)}| + 1, \dots, |C|$ . The algorithm succeeds:

**Theorem 4.6.** *Let  $\lfloor \delta_C/2 \rfloor > \delta$ . In Algorithm 4.5 let the input  $S$  be sufficient. Then for the output  $\hat{C}^{(n)}$  it holds a.s. as  $n \rightarrow \infty$  that*

$$|\hat{C}^{(n)}| \longrightarrow |C| \quad \text{and} \quad \limsup_{n \rightarrow \infty} |\hat{c}_u^{(n)} - c_u| \leq \delta - 1 \quad \text{for all } u = 1, \dots, |C|.$$

Location estimation is correct up to  $\delta - 1$ . The choice  $\delta = 1$  states strong consistency. Recall that  $\lfloor \delta_C/2 \rfloor > \delta$  is needed for sufficiency of  $S = S_g$  in Lemma 4.4. Also it implies  $\delta_C > 2(\delta - 1)$ , i.e., neighboring change points should be separated by more than the worst errors of their estimators. The proof applies Proposition 4.3 for the estimation of  $C$ , and Corollary 3.2 for correct breaking.

## 5 Practical aspects

**Parameter choice** We give recommendations for the choice of  $S$ ,  $\kappa$  and  $\delta$  in practice, where  $n = 1$ . Then, the threshold is  $\kappa \cdot n^\beta = \kappa$ , i.e.,  $\beta$  is redundant.

1. Choice of  $\kappa$ :  $\kappa$  can be chosen as the rejection threshold of a test for  $H_0 : C = \emptyset$ : For  $H_0$  Proposition 3.4 implies weak convergence of  $\sup_{t,h \in \Delta_\delta} |D_{t,h}^{(n)}| \rightarrow \sup_{(t,h) \in \Delta_\delta} |L_{(t,h)}|$ , and we choose  $\kappa$  as the  $(1 - \alpha)$ -quantile of the limit distribution (e.g., significance level  $\alpha = 0.01$ ), which can be derived in simulations, compare e.g., Messer et al. (2014). If  $|\hat{C}^{(1)}| > 0$ , then  $H_0$  is rejected at level  $\leq \alpha$ , as the maximum w.r.t. a path is bounded by the supreme over  $\Delta_\delta$ .
2. Choice of  $S$ : Lemma 4.4 states sufficiency of  $S = S_g$  if  $g \leq \lfloor \delta_C/2 \rfloor$  (in case  $\delta < \lfloor \delta_C/2 \rfloor$ ). Thus, if  $\delta_C$  is known it is reasonable to choose  $g = \lfloor \delta_C/2 \rfloor$  as  $g$  large reduces computational complexity. If  $\delta_C$  is unknown, we set  $g = \delta$  or even smaller if computational complexity allows for.
3. Choice of  $\delta$ : We recommend  $\delta = 20$ : by construction, asymptotic considerations imply an increase of the double windows. For  $n \rightarrow \infty$ , weakly  $D_{t,h}^{(n)} \rightarrow L_{t,h} \sim N(0, 1)$  for all  $(t, h) \in \Delta_\delta$ , but for  $n = 1$  small  $h$  means less observations and the approximation via  $N(0, 1)$  is harder to justify. Practically, for tiny  $h$  there is high variability in  $\hat{\mu}_j$  and  $\hat{\sigma}_j^2$  and thus  $D_{t,h}^{(1)}$  is likely to take extreme values even if no change is involved, resulting in false positives. Thus,  $\delta$  should be bounded from below. Figure 9 shows simulations for the probability that  $\mathbb{P}(|\hat{C}^{(1)}| > 0)$  if  $C = \emptyset$  (rejection probability under  $H_0$ ), for both  $\alpha = 0.05$  and  $\alpha = 0.01$ , depending on  $\delta$ . Over a variety of distributions, including normal, exponential, gamma, binomial and Poisson, for  $\delta \geq 20$  the  $\alpha$ -level is kept throughout.

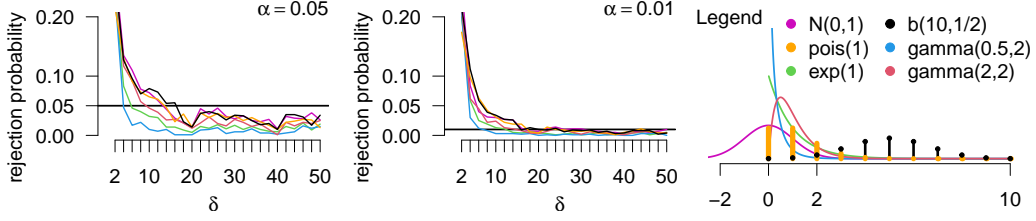


Figure 9: Rejection probability under  $C = \emptyset$  (1000 simulations) depending on  $\delta \in \{2, 4, \dots, 50\}$ .  $T = 1000$ , left:  $\alpha = 5\%$ , right:  $\alpha = 1\%$ . Six distributions color coded:  $N(0, 1)$  (magenta),  $Pois(1)$  (orange),  $exp(1)$  (green),  $b(10, 1/2)$  (black),  $gamma(0.5, 2)$  (blue) and  $gamma(2, 2)$  (red). Right: Legend.

In the following we use  $\delta = g = 20$  and  $\kappa$  is derived in simulations for  $\alpha = 0.01$ .

**Simulation studies** We evaluate the performance of MSCP in simulation studies. Throughout it is  $T = 1000$  and  $|C| = 5$ . We consider different scenarios of locations  $c_u \in C$  and parameters  $\mu_u$  and  $\sigma_u$ , given in Table 10. Scenarios 1 - 3 differ in  $C$ : in 1 it is  $c_{u+1} - c_u = 200$ , and in 2 it is  $c_{u+1} - c_u = 100$  throughout, and 3 describes a multiscale setup where  $c_1 = 200$  is well separated and for the others it is  $c_{u+1} - c_u = 50$ . For each choice of  $C$  we then consider different effects by altering both changes in  $\mu_u$  and in  $\sigma_u$ . E.g., 1a states certain  $\mu_u$  which are halved in 1c. Also, in 1a it is  $\sigma_u = 1$  constant, while in 1b the  $\sigma_u$  alter between 1 and 2. For each scenario we consider different distributions: A.  $N(\mu, \sigma^2)$  (normal), B.  $gamma(s, \lambda)$  (gamma), C.  $Poi(\lambda)$  (Poisson), D.  $b(10, p)$  (binomial,  $n = 10$  fix), and E. is a combination of the previous that changes between the six sections using A., B., C., D., A., B. (mix). Note that for  $Poi(\lambda)$  and  $b(10, p)$  the formulation of  $\sigma_u$  can be disregarded as it follows from  $\mu_u$ , and also if distributions coincide due to equality of  $\mu_u$  as e.g., in 1a and 1b, they are presented only once.

Scenario	$C$	$\mu_u$	$\sigma_u$
1a	100, 300, 500, 700, 900	1, 4, 1, 8, 1, 4	1, 1, 1, 1, 1, 1
1b	100, 300, 500, 700, 900	1, 4, 1, 8, 1, 4	1, 2, 1, 2, 1, 2
1c	100, 300, 500, 700, 900	0.5, 2, 0.5, 4, 0.5, 2	1, 1, 1, 1, 1, 1
2a	300, 400, 500, 600, 700	1, 4, 1, 8, 1, 4	1, 1, 1, 1, 1, 1
2b	300, 400, 500, 600, 700	1, 4, 1, 8, 1, 4	1, 2, 1, 2, 1, 2
2c	300, 400, 500, 600, 700	0.5, 2, 0.5, 4, 0.5, 2	1, 1, 1, 1, 1, 1
3a	200, 500, 550, 600, 750	1, 4, 1, 8, 1, 4	1, 1, 1, 1, 1, 1
3b	200, 500, 550, 600, 750	1, 4, 1, 8, 1, 4	1, 2, 1, 2, 1, 2
3c	200, 500, 550, 600, 750	0.5, 2, 0.5, 4, 0.5, 2	1, 1, 1, 1, 1, 1
3d	200, 500, 550, 600, 750	0.5, 2, 0.5, 4, 0.5, 2	1, 2, 1, 2, 1, 2
3e	200, 500, 550, 600, 750	1, 2, 4, 8, 4, 2	1, 1, 1, 1, 1, 1

Figure 10: Scenarios of  $C$ ,  $\mu$  and  $\sigma$  considered in simulations.

For each scenario we run 1000 simulations, i.e., there are  $1000 \cdot |C| = 5000$  change points in total. W.r.t. a critical value  $\mathcal{V}$  we classify an estimate  $\hat{c}$  as correct if  $m_{\hat{c}} := \min_{c \in C} |\hat{c} - c| \leq \mathcal{V}$ . Let  $\hat{C}_{\mathcal{V}}$  denote the set of all correct estimates w.r.t.  $\mathcal{V}$ . Then  $\hat{C}_T$  is the set of all estimates. We compute  $|\hat{C}_T|$ , and for  $\mathcal{V} \in \{10, 5, 2\}$  both  $|\hat{C}_{\mathcal{V}}|$  and the mean absolute deviation  $M_{\mathcal{V}} := |C_{\mathcal{V}}|^{-1} \sum_{\hat{c} \in C_{\mathcal{V}}} m_{\hat{c}}$ . The results, depending on the scenarios and distributions, are reported in tables 11 - 13

Scenario	Distribution	$ \hat{C}_T $	$ \hat{C}_{10} , M_{10}$	$ \hat{C}_5 , M_5$	$ \hat{C}_2 , M_2$
1a	normal	5005	5000, 0.1	5000, 0.1	4994, 0.1
1a	gamma	5002	5000, 0.1	5000, 0.1	4993, 0.1
1a	Poisson	5005	5000, 0.4	4993, 0.3	4905, 0.3
1a	binomial	5005	5000, 0.2	4998, 0.2	4954, 0.2
1a	mix	5001	5000, 0.1	5000, 0.1	4993, 0.1
1b	normal	5001	4998, 0.3	4993, 0.3	4906, 0.2
1b	gamma	5000	5000, 0.3	4997, 0.3	4909, 0.2
1b	mix	5004	5000, 0.3	4999, 0.3	4906, 0.2
1c	normal	4951	4935, 0.5	4912, 0.5	4698, 0.4
1c	gamma	4953	4932, 0.4	4925, 0.4	4823, 0.3
1c	Poisson	4640	4626, 0.6	4600, 0.6	4370, 0.5
1c	binomial	4891	4883, 0.6	4858, 0.5	4642, 0.4
1c	mix	4936	4929, 0.6	4903, 0.5	4707, 0.4

Figure 11: Simulation results for scenarios 1a-c.

Scenario	Distribution	$ \hat{C}_T $	$ \hat{C}_{10} , M_{10}$	$ \hat{C}_5 , M_5$	$ \hat{C}_2 , M_2$
2a	normal	5002	5000, 0.1	5000, 0.1	4993, 0.1
2a	gamma	5002	5000, 0.1	5000, 0.1	4988, 0.1
2a	Poisson	5005	5000, 0.3	4998, 0.3	4908, 0.3
2a	binomial	5002	5000, 0.2	5000, 0.2	4958, 0.2
2a	mix	5002	5000, 0.1	5000, 0.1	4989, 0.1
2b	normal	5002	4998, 0.3	4995, 0.3	4914, 0.2
2b	gamma	5003	5000, 0.3	4998, 0.3	4928, 0.2
2b	mix	5008	5000, 0.3	4998, 0.3	4935, 0.2
2c	normal	4884	4873, 0.5	4855, 0.5	4663, 0.4
2c	gamma	4906	4870, 0.4	4863, 0.3	4766, 0.3
2c	Poisson	4553	4541, 0.7	4520, 0.6	4285, 0.5
2c	binomial	4847	4841, 0.5	4828, 0.5	4647, 0.4
2c	mix	4926	4920, 0.5	4902, 0.5	4720, 0.4

Figure 12: Simulation results for scenarios 2a-c.

We summarize the results. In the well-posed scenarios 1a-c we obtain precise estimates:  $\hat{C}_T$  is close to 5000 over all scenarios and distributions. Notably, in 1a it is exactly  $\hat{C}_{10} = 5000$  throughout, and  $\hat{C}_5 = 5000$  for three distributions. Also, the strict measure  $\hat{C}_2$  reveals precise results. In 1b we consider varying  $\sigma_u$ , but the estimates remain similarly precise. In 1c we have jump sizes halved but still detect a high number of change points at reasonable precision over all distributions. Setup 2a-c is again well-posed in the sense that results are strong: 2a and 2b are pretty similar to 1a and 1b, and in 2c there is some loss over 1c. In setup 3a-c performance is reduced a bit as compared to 2a-c due to closer distances. Nevertheless, we obtain about 5000 estimates at precise location for 3a and 3b, and about 4800 estimates for 3c (Poisson reduced to  $\approx 4400$ ). In scenario 3d we reduced the effects w.r.t. both smaller jump sizes and higher variances, and we now see performance losses as we obtain only around 3000 estimates. But note that e.g., for  $c_6$  it is  $\mu_6 - \mu_5 = 1.5$  with  $\sigma_6 = 2$  which is reasonably hard to be detected, also taking into account the smaller spacings between  $c_u$ . Despite the reduced number,

Scenario	Distribution	$ \hat{C}_T $	$ \hat{C}_{10} , M_{10}$	$ \hat{C}_5 , M_5$	$ \hat{C}_2 , M_2$
3a	normal	5004	4990, 0.3	4910, 0.2	4846, 0.1
3a	gamma	5002	4990, 0.3	4879, 0.2	4828, 0.1
3a	Poisson	4942	4876, 0.9	4580, 0.5	4334, 0.3
3a	binomial	5005	4965, 0.6	4787, 0.3	4652, 0.2
3a	mix	5000	4991, 0.3	4901, 0.1	4857, 0.1
3b	normal	4988	4928, 0.8	4657, 0.4	4478, 0.3
3b	gamma	4995	4939, 0.8	4689, 0.4	4482, 0.2
3b	mix	5001	4947, 0.6	4789, 0.3	4638, 0.2
3c	normal	4814	4703, 1.3	4286, 0.7	3936, 0.4
3c	gamma	4820	4749, 1.2	4334, 0.5	4095, 0.3
3c	Poisson	4387	4249, 1.5	3845, 0.8	3480, 0.5
3c	binomial	4750	4644, 1.5	4146, 0.7	3809, 0.4
3c	mix	4856	4756, 1.3	4334, 0.7	3990, 0.4
3d	normal	3093	2946, 1.6	2620, 0.8	2380, 0.5
3d	gamma	2962	2842, 1.8	2472, 0.8	2193, 0.4
3d	mix	2896	2804, 1.4	2548, 0.7	2296, 0.4
3e	normal	4680	4566, 1.1	4257, 0.5	3984, 0.3
3e	gamma	4735	4620, 1.0	4302, 0.5	4046, 0.3
3e	Poisson	3411	3085, 2.3	2584, 1.2	2154, 0.6
3e	binomial	4129	3883, 1.8	3346, 0.8	2959, 0.4
3e	mix	4220	4014, 1.8	3452, 0.8	3070, 0.4

Figure 13: Simulation results for scenarios 3a-e.

note that precision for detected estimates is kept high. Scenario 3e is another example with different jump sizes resulting in a good overall outcome, but slightly weaker than 3a as effects are reduced similar to 3c. Overall, MSCP yields reliable results over different scenarios of change points and effects: both the number and the locations are reliably estimated. Notably, performance is also kept over different distributions and regardless of changes in variance.

**Data example** We apply MSCP to the daily number of new COVID-19 cases in Zimbabwe between 2020/3/3 and 2020/12/14, yielding  $T = 269$  time stamps, as reported in (Ministry of Health and Child Care of Zimbabwe, 2021). The result is depicted in Figure 14.

Four change points were estimated,  $\hat{C} = \{68, 110, 173, 241\}$ , yielding parameter estimates  $\hat{\mu}_u \approx 1, 17, 104, 22, 85$  and  $\hat{\sigma}_u \approx 1, 18, 83, 16, 35$ . The segmentation closely aligns with visual inspection. Note that an increase in mean is accompanied with an increase in variance, and vice versa. In each section, serial correlation proves to be small (i.e.,  $\leq 0.2$ , while in the last section for the first time lag it is  $\approx 0.4$  and negligible for higher lags).

## 6 Appendix

**Proof of Lemma 3.1:** W.l.o.g. let  $j = \ell$ . For  $\hat{\mu}_\ell^{(k)}$  first let  $C = \emptyset$  where we need to show  $n^v \cdot (\hat{\mu}_\ell^{(k)} - \mu^{(k)})_{(t,h)} \rightarrow (0)_{(t,h)}$  a.s. as  $n \rightarrow \infty$ . We show some uniform convergence



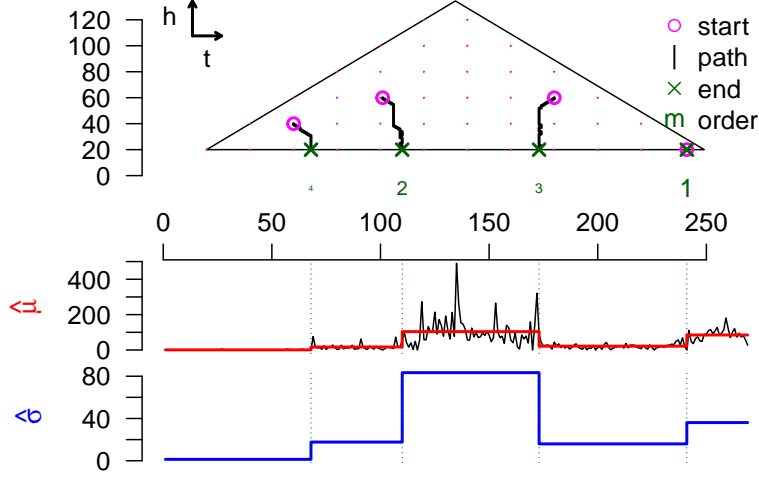


Figure 14: Analysis of daily COVID-19 infections in Zimbabwe, from 2020/3/3 to 2020/12/14.

w.r.t  $[0, T]$  and then extend considerations to  $\Delta_\delta$ . It holds a.s. as  $n \rightarrow \infty$

$$n^v \cdot \sup_{t \in [0, T]} \left| \frac{1}{n} \sum_{i=1}^{\lfloor nt \rfloor} X_i^k - t\mu^{(k)} \right| \rightarrow 0, \quad \text{for } v \in \begin{cases} (-\infty, 1/2), & \text{if } k = 1, \\ (-\infty, 1/2) \cap (-\infty, p/(p+2)], & \text{if } k = 2. \end{cases} \quad (13)$$

For this, first apply Marcinkiewicz-Zygmund (MZ)-SLLN to  $(X_i)_i$  and  $(X_i^2)_i$ : For  $(X_i)_i$  note that for any  $\alpha \in (0, 2)$  it is  $\mathbb{E}[|X_i|^\alpha] < \infty$ , and thus for  $k = 1$  a.s. as  $n \rightarrow \infty$

$$n^{(\alpha-1)/\alpha} \cdot \left( \frac{1}{n} \sum_{i=1}^n X_i^k - \mu^{(k)} \right) = n^{-1/\alpha} \cdot \left( \sum_{i=1}^n X_i^k - n\mu^{(k)} \right) \rightarrow 0. \quad (14)$$

For the squares  $(X_i^2)_i$  we choose  $\alpha \in (0, (2+p)/2]$  if  $p < 2$  and  $\alpha \in (0, 2)$  if  $p \geq 2$ . Then  $\mathbb{E}[|X_i^2|^\alpha] < \infty$  and thus (14) applies for  $k = 2$ . As  $(\alpha - 1)/\alpha \leq p/(2+p)$  if  $p < 2$ , and  $(\alpha - 1)/\alpha < 1/2$  if  $p \geq 2$ , we obtain for  $k = 1, 2$  a.s. as  $n \rightarrow \infty$

$$n^v \cdot \left( \frac{1}{n} \sum_{i=1}^n X_i^k - \mu^{(k)} \right) \rightarrow 0, \quad \text{for } v \in \begin{cases} (-\infty, 1/2), & \text{if } k = 1, \\ (-\infty, 1/2) \cap (-\infty, p/(p+2)], & \text{if } k = 2. \end{cases} \quad (15)$$

For uniform convergence in (13) we discretize time and apply (15), a.s. as  $n \rightarrow \infty$

$$\begin{aligned} n^v \cdot \sup_{0 \leq t \leq T} \left| \frac{1}{n} \sum_{i=1}^{\lfloor nt \rfloor} X_i^k - t\mu^{(k)} \right| &\leq n^v \cdot \sup_{0 \leq t \leq T} \left| \frac{1}{n} \sum_{i=1}^{\lfloor nt \rfloor} X_i^k - \frac{\lfloor nt \rfloor}{n} \mu^{(k)} \right| + r_n \\ &= n^v \cdot \max_{m \in \{1, 2, \dots, nT\}} \left| \frac{1}{n} \sum_{i=1}^m X_i^k - \frac{m}{n} \mu^{(k)} \right| + r_n \rightarrow 0, \end{aligned}$$

as  $r_n := n^v \cdot \sup_{t \in [0, T]} |t - \lfloor nt \rfloor / n| \mu^{(k)} \leq n^v \cdot (1/n) \mu^{(k)} \rightarrow 0$  as  $n \rightarrow \infty$ , and for  $\varepsilon > 0$

$$\begin{aligned} & n^v \cdot \max_{m \in \{1, 2, \dots, nT\}} \left| \frac{1}{n} \sum_{i=1}^m X_i^k - \frac{m}{n} \mu^{(k)} \right| \\ & \leq n^v \cdot \frac{1}{n} \max_{m \leq m_0} \left| \sum_{i=1}^m X_i^k - m \mu^{(k)} \right| + T^{1-v} \max_{m_0 < m \leq nT} \left( \frac{m}{nT} \right)^{1-v} m^v \cdot \left| \frac{1}{m} \sum_{i=1}^m X_i^k - \mu^{(k)} \right| \leq \varepsilon \end{aligned}$$

a.s. for  $n$  large enough, as the maximum in the first summand is independent from  $n$ , and for the second summand note  $(m/nT)^{1-v} \leq 1$  and (15) yields that for almost every realization we find  $m_0 \in \mathbb{N}$  such that  $m^v \cdot |(1/m) \sum_{i=1}^m X_i^k - \mu^{(k)}| < T^{v-1} \varepsilon / 2$  for all  $m > m_0$ . Thus, (13) holds. Now we consider  $\Delta_\delta$ . As  $0 \leq t - h \leq T$  for all  $(t, h) \in \Delta_\delta$ , (13) yields a.s. as  $n \rightarrow \infty$

$$n^v \cdot \sup_{(t, h) \in \Delta_\delta} \left| \frac{1}{n} \sum_{i=1}^{\lfloor nt \rfloor} X_i^k - t \mu^{(k)} \right| \rightarrow 0 \quad \text{and} \quad n^v \cdot \sup_{(t, h) \in \Delta_\delta} \left| \frac{1}{n} \sum_{i=1}^{\lfloor n(t-h) \rfloor} X_i^k - (t-h) \mu^{(k)} \right| \rightarrow 0,$$

We include the factor  $1/h \geq 2/T > 0$  and obtain in  $(\mathcal{D}_{\mathbb{R}}[\Delta_\delta], \|\cdot\|_\infty)$  a.s. as  $n \rightarrow \infty$

$$\begin{aligned} & n^v \cdot (\hat{\mu}_\ell^{(k)} - \mu^{(k)})_{(t, h)} \\ & = n^v \cdot \left[ \left( \frac{1}{nh} \sum_{i=1}^{\lfloor nt \rfloor} X_i^k - \frac{t}{h} \mu^{(k)} \right) - \left( \frac{1}{nh} \sum_{i=1}^{\lfloor n(t-h) \rfloor} X_i^k - \frac{t-h}{h} \mu^{(k)} \right) \right]_{(t, h)} \rightarrow (0)_{(t, h)}. \end{aligned} \tag{16}$$

Now let  $C \neq \emptyset$ . We segment  $(t-h, t]$  according to  $C$  and find  $\hat{\mu}_\ell^{(k)} - \mu^{(k)}$  as

$$\sum_{u=1}^{\lfloor C_\ell \rfloor + 1} \left( \left[ \frac{\lfloor nc_{\ell, u} \rfloor - \lfloor nc_{\ell, u-1} \rfloor}{nh} \cdot \frac{1}{\lfloor nc_{\ell, u} \rfloor - \lfloor nc_{\ell, u-1} \rfloor} \sum_{i=\lfloor nc_{\ell, u-1} \rfloor + 1}^{\lfloor nc_{\ell, u} \rfloor} X_i^k \right] - \frac{d_{\ell, u}}{h} \cdot \mu_{\ell, u}^{(k)} \right). \tag{17}$$

The  $u$ -th summand refers to a subsection that relates to the error sequence  $(Z_{u, i})_{i=1, 2, \dots}$  and in which  $X_i$  equals  $\mu_u + \sigma_u \cdot Z_{u, i}$ . From (16) we conclude a.s. as  $n \rightarrow \infty$

$$n^v \cdot \sup_{1 \leq d \leq t \leq T} \left| \frac{1}{\lfloor nd \rfloor} \sum_{i=\lfloor n(t-d) \rfloor + 1}^{\lfloor nt \rfloor} (\mu_u + \sigma_u \cdot Z_{u, i})^k - \mu_u^{(k)} \right| \rightarrow 0, \tag{18}$$

which states uniform convergence w.r.t all subintervals of varying length  $d$ . When including the factor  $d/h \geq 1$  and summing over all  $u$ , the expression still vanishes a.s. as  $n \rightarrow \infty$ , and it states an upper bound for  $n^v \cdot \sup_{(t, h) \in \Delta_\delta} |\hat{\mu}_\ell^{(k)} - \tilde{\mu}_\ell^{(k)}|$ .

Regarding  $\hat{\sigma}_\ell^2$  we decompose in the  $u$ -th subsection  $(X_i - \hat{\mu}_\ell)^2 = (X_i - \mu_{\ell, u})^2 - 2(X_i - \mu_{\ell, u})(\hat{\mu}_\ell - \mu_{\ell, u}) + (\hat{\mu}_\ell - \mu_{\ell, u})^2$ . Averages in the subsection tend to  $\sigma_{\ell, u}^2 + 0 + (\tilde{\mu}_\ell - \mu_{\ell, u})^2$ , and summation over subsections yields a.s. as  $n \rightarrow \infty$  that  $n^v \cdot \sup_{(t, h) \in \Delta_\delta} |\hat{\sigma}_\ell^2 - \tilde{\sigma}_\ell^2| \rightarrow 0$ , as before using MZ-SLLN and discretization arguments.  $\square$

**Proof of Lemma 3.3:** Continuity is inherited from the limits in (5) and (6). W.l.o.g. consider  $c_1 =: c$ . As  $v_{t, h} \geq 1$  with equality at  $c$  it is  $v_{t, h} \cdot |d_{t, h}^{(n)}| \geq |d_{t, h}^{(n)}|$ .  $\tilde{\mu}_r - \tilde{\mu}_\ell$  has the shape of a hat: it is zero outside the  $h$ -neighborhood of  $c$ , it is  $\mu_2 - \mu_1$  at  $c$ , and it is linearly interpolated in between.  $\tilde{\sigma}_r^2 + \tilde{\sigma}_\ell^2$  is  $2\sigma_1^2$  left of  $c - h$ , and  $2\sigma_2^2$  right of  $c + h$ , and

linearly interpolated in between. Thus, in the  $h$ -neighborhood of  $c$  the root  $(\tilde{\sigma}_r^2 + \tilde{\sigma}_\ell^2)^{1/2}$  is constant if  $\sigma_2^2 = \sigma_1^2$ , it is strictly convex if  $\sigma_2^2 > \sigma_1^2$  and strictly concave if  $\sigma_2^2 < \sigma_1^2$ . As the numerator is piecewise linear, i.e., of order  $t$ , and the denominator of order  $t^{1/2}$ , the statements about the curvatures of  $v_{t,h} \cdot d_{t,h}^{(n)}$  hold true. We now turn to  $d_{t,h}^{(n)}$ . We represent  $\tilde{\sigma}_j^2$  through  $\tilde{\sigma}_j^2$  plus errors

$$\tilde{\sigma}_j^2 = \sum_{u=1}^2 \frac{d_u}{h} \cdot [\sigma_u^2 + (\tilde{\mu}_j - \mu_u)^2] = \tilde{\sigma}_j^2 + \frac{d_1 d_2}{h^2} \cdot (\mu_2 - \mu_1)^2,$$

for  $j \in \{\ell, r\}$ , i.e., we find the error as  $e_j^2 := [d_1 d_2 / h^2] (\mu_2 - \mu_1)^2$ . We abbreviated  $d_u := d_{j,u}$ . Note that  $e_\ell^2 = e_r^2$ , and set  $x := d_1 / h$  and  $d_2 / h = (1 - h) / h = (1 - x)$  with  $x \in [0, 1]$ , which yields a representation through the proportions of the window left and right of  $c$ . Note that the error  $e_j^2 = x(1 - x) \cdot (\mu_2 - \mu_1)^2$  is quadratic and maximal for  $x = 1/2$ , thus taking the value  $(\mu_2 - \mu_1)^2 / 4$ , which is plausible as half of the window refers to the left and the other half to the right population. Within both  $[c - h, c]$  and  $(c, c + h]$  it holds that  $\tilde{\mu}_r - \tilde{\mu}_\ell$  is linear in  $x$  and the denominator of  $d_{t,h}^{(n)}$  is now the root of first function  $\tilde{\sigma}_r^2 + \tilde{\sigma}_\ell^2$  which is linear in  $x$  plus second the quadratic error  $e_j^2$ . W.l.o.g. we consider  $t \in [c - h, c]$  where the right window contains  $c$ . Then we find  $d_{t,h}^{(n)}$  as a function  $f$  of  $x$  as

$$f(x) = \sqrt{nh} \cdot \frac{(\mu_2 - \mu_1) \cdot x}{\sqrt{[(\sigma_2^2 - \sigma_1^2) \cdot x + 2\sigma_1^2] + [(\mu_2 - \mu_1)^2 \cdot x \cdot (1 - x)]}}, \quad x \in [0, 1],$$

for all valid  $h \in (\delta, T/2]$ , which yields the derivative w.r.t.  $x$

$$f'(x) = \sqrt{nh} \cdot (\mu_2 - \mu_1) \cdot \frac{2^{-1}[(\sigma_2^2 - \sigma_1^2) + (\mu_2 - \mu_1)^2] \cdot x + 2\sigma_1^2}{[(\sigma_2^2 - \sigma_1^2) \cdot x + 2\sigma_1^2 + (\mu_2 - \mu_1)^2 \cdot x \cdot (1 - x)]^{3/2}}.$$

In (19) we see that the fraction is positive and thus  $f'(x) > 0$  if  $\mu_2 > \mu_1$  and  $f'(x) < 0$  if  $\mu_2 < \mu_1$ , which gives (8). To bound  $|f'(x)|$  we find the numerator  $\geq 2^{-1}[\sigma_2^2 + 3\sigma_1^2 + (\mu_2 - \mu_1)^2] \wedge 2\sigma_1^2$  and for the denominator we get  $(\sigma_2^2 - \sigma_1^2)x + 2\sigma_1^2 \leq 2(\sigma_2^2 \vee \sigma_1^2)$  and  $x(1 - x) \leq 1/4$ , such that

$$\begin{aligned} |f'(x)| &\geq \sqrt{nh} \cdot |\mu_2 - \mu_1| \cdot \frac{2^{-1}[\sigma_2^2 + 3\sigma_1^2 + (\mu_2 - \mu_1)^2] \wedge 2\sigma_1^2}{[2(\sigma_2^2 \vee \sigma_1^2) + (\mu_2 - \mu_1)^2 / 4]^{3/2}} \\ &\geq \sqrt{nh} \cdot |\mu_2 - \mu_1| \cdot \frac{2(\sigma_2^2 \wedge \sigma_1^2)}{[2(\sigma_2^2 \vee \sigma_1^2) + (\mu_2 - \mu_1)^2 / 4]^{3/2}} > 0. \end{aligned} \quad (19)$$

In the second inequality we omitted  $(\mu_2 - \mu_1)^2 \geq 0$  and used that  $2\sigma_1^2 < 2^{-1}[\sigma_2^2 + 3\sigma_1^2]$  iff  $\sigma_1^2 < \sigma_2^2$ . This is the lower bound in (9). For the upper bound we find the numerator  $\leq 2^{-1}[\sigma_2^2 + 3\sigma_1^2 + (\mu_2 - \mu_1)^2] \vee 2\sigma_1^2 \leq 2(\sigma_2^2 \vee \sigma_1^2) + (\mu_2 - \mu_1)^2$ , and for the denominator we mention  $(\sigma_2^2 - \sigma_1^2)x + 2\sigma_1^2 \geq 2(\sigma_2^2 \wedge \sigma_1^2)$  such that

$$|f'(x)| \leq \sqrt{nh} \cdot |\mu_2 - \mu_1| \cdot \frac{2(\sigma_2^2 \vee \sigma_1^2) + (\mu_2 - \mu_1)^2}{[2(\sigma_2^2 \wedge \sigma_1^2)]^{3/2}},$$

which completes (9). □

**Proof of Proposition 3.4:** Donsker's theorem yields in  $(\mathcal{D}_{\mathbb{R}}[0, T], \|\cdot\|_{\infty})$  as  $n \rightarrow \infty$

$$\left[ \frac{1}{\sigma\sqrt{n}} \cdot \sum_{i=1}^{\lfloor nt \rfloor} (X_i - \mu) \right]_t \xrightarrow{d} (W_t)_t. \quad (20)$$

Define a continuous map  $\varphi$  from  $(\mathcal{D}_{\mathbb{R}}[0, T], \|\cdot\|_{\infty})$  to  $(\mathcal{D}_{\mathbb{R}}[\Delta_{\delta}], \|\cdot\|_{\infty})$  via

$$\varphi : (f(t))_t \rightarrow \left( \frac{[f(t+h) - f(t)] - [f(t) - f(t-h)]}{\sqrt{2h}} \right)_t,$$

and apply  $\varphi$  on (20). The continuous mapping yields in  $(\mathcal{D}_{\mathbb{R}}[\Delta_{\delta}], \|\cdot\|_{\infty})$  as  $n \rightarrow \infty$

$$\left( \frac{1}{(2\sigma^2 nh)^{1/2}} \left[ \sum_{i=\lfloor nt \rfloor + 1}^{\lfloor n(t+h) \rfloor} X_i - \sum_{i=\lfloor n(t-h) \rfloor + 1}^{\lfloor nt \rfloor} X_i \right] \right)_t \xrightarrow{d} (L_{t,h})_t,$$

where the constant  $\mu$  vanishes. Now by replacing  $2\sigma^2$  by  $\hat{\sigma}_r^2 + \hat{\sigma}_\ell^2$  and using Lemma 3.1 and Slutsky's theorem weak convergence of  $(D_{t,h}^{(n)})_{(t,h) \in \Delta_{\delta}}$  follows.  $\square$

**Proof of Lemma 4.2:** Within  $A_u$  the slope of  $(n^{-1/2} \cdot |d_{t,h}^{(n)}|)_t$  is positive left of  $c_u$  and negative right of it, see Lemma 3.3. Thus,  $|t_s(k) - c_u| = |t_s - c_u| - (k+1) \Leftrightarrow |t_s - c_u| \geq k+1$  and (12) holds true. The path ends after  $h_s - \delta$  steps, i.e.,  $t_e = c_u \Leftrightarrow |t_s - c_u| \leq h_s - \delta + 1 \Leftrightarrow (t_s, h_s) \in B_u$ . Further,  $(t_s, h_s) \in A_u$  implies  $|t_s - c_u| \leq h_s$  (double window overlaps  $c_u$ ), and thus  $(t_s, h_s) \in A_u \setminus B_u$  implies  $|t_s - c_u| \in \{h_s - \delta + 2, \dots, h_s\}$ , hence  $|t_e - c_u| = |t_s - c_u| - (h_s - \delta + 1) \in \{1, \dots, \delta\}$ .  $\square$

**Proof of Proposition 4.3** From Corollary 3.2 we obtain a.s. as  $n \rightarrow \infty$

$$\sup_{(t,h) \in \Delta_{\delta}} \left| |n^{-1/2} \cdot D_{t,h}^{(n)}| - |d_{t,h}^{(1)}| \right| \rightarrow 0. \quad (21)$$

On  $A_u$  (excluding  $t = c_u$ ) a lower bound for the derivative of  $(|d_{t,h}^{(1)}|)_t$  is given through  $\kappa_a \delta^{1/2} > 0$ , see Lemma 3.3. Thus, for any  $\varepsilon > 0$  it is

$$|d_{t,h}^{(1)}| - |d_{t-\varepsilon,h}^{(1)}| \geq \kappa_a \delta^{1/2} \varepsilon, \text{ if } t \leq c_u, \quad \text{and} \quad |d_{t,h}^{(1)}| - |d_{t+\varepsilon,h}^{(1)}| \geq \kappa_a \delta^{1/2} \varepsilon, \text{ if } t > c_u, \quad (22)$$

provided that  $(t, h)$ ,  $(t - \varepsilon, h)$ ,  $(t + \varepsilon, h)$  lie in  $A_u$ . Consider the initializing step of the path,  $k = 0$ . Both  $\hat{t}_s^{(n)}(k)$  and  $t_s(k)$  take a value in  $\{t_s - 1, t_s, t_s + 1\} \cap \Delta_{\delta}$ . As  $\hat{t}_s^{(n)}(k)$  is a maximizer defined via  $|D_{t,h}^{(n)}|$  we obtain  $|n^{-1/2} \cdot D_{\hat{t}_s^{(n)}(k), h-k}^{(n)}| \geq |n^{-1/2} \cdot D_{t_s(k), h-k}^{(n)}| \rightarrow |d_{t_s(k), h-k}^{(1)}|$  a.s. as  $n \rightarrow \infty$ , where the convergence follows from (21), i.e.,

$$|n^{-1/2} \cdot D_{\hat{t}_s^{(n)}(k), h-k}^{(n)}| \geq |d_{t_s(k), h-k}^{(1)}| + o_{a.s.}(1). \quad (23)$$

From this we bound

$$\begin{aligned}
|d_{t_s(k),h-k}^{(1)}| - |d_{\hat{t}_s^{(n)}(k),h-k}^{(1)}| + o_{a.s.}(1) &\leq |n^{-1/2} \cdot D_{\hat{t}_s^{(n)}(k),h-k}^{(n)}| - |d_{\hat{t}_s^{(n)}(k),h-k}^{(1)}| + o_{a.s.}(1) \\
&\leq \left| n^{-1/2} \cdot D_{\hat{t}_s^{(n)}(k),h-k}^{(n)} - d_{\hat{t}_s^{(n)}(k),h-k}^{(1)} \right| + o_{a.s.}(1) \\
&\leq \sup_{(t,h) \in \Delta_\delta} \left| n^{-1/2} \cdot D_{t,h}^{(n)} - d_{t,h}^{(1)} \right| + o_{a.s.}(1) \xrightarrow{a.s.} 0. \quad (24)
\end{aligned}$$

In the first inequality we used (23), in the second the triangle inequality, and the convergence follows from (21). The estimator  $\hat{t}_s^{(n)}(k)$  is now tied to the nonrandom function via  $d_{\hat{t}_s^{(n)}(k),h-k}^{(1)}$ , and (22) brings us from the function to the estimator. Let  $\varepsilon > 0$ . Then almost everywhere it holds that if  $|t_s(k) - \hat{t}_s^{(n)}(k)| > \varepsilon$  i.o., thus  $|d_{t_s(k),h-k}^{(1)}| - |d_{\hat{t}_s^{(n)}(k),h-k}^{(1)}| > \varepsilon \kappa_a \delta^{1/2}$  i.o. But as the latter only occurs finitely often it is  $t_s(k) = \hat{t}_s^{(n)}(k)$  a.s. for  $n$  large. Iteratively, this extends for all  $k = 1, 2, \dots, h - \delta$ , i.e., eventually the paths w.r.t.  $D_{t,h}^{(n)}$  and  $d_{t,h}^{(1)}$  coincide a.s.  $\square$

**Proof of Lemma 4.4:** From  $\delta < \lfloor \delta_C/2 \rfloor$  conclude that  $A_u$  contains a square  $\mathcal{S}$  with horizontal and vertical edges of length  $\lfloor \delta_C/2 \rfloor$ : choose the center of  $\mathcal{S}$  as  $(c_u, \delta_C)$ . In fact, the right corners of  $\mathcal{S}$  may only be adjacent to  $A_u$ . Nevertheless,  $\mathcal{S} \cap S_{\lfloor \delta_C/2 \rfloor} \neq \emptyset$ , and thus  $\mathcal{S} \cap S_g \neq \emptyset$  for  $g \leq \lfloor \delta_C/2 \rfloor$ .  $\square$

**Proof of Theorem 4.6:** For  $(t_s, h_s) \in S$  set  $\hat{t}_{e_s}^{(n)} := \hat{t}_e^{(n)}$ , making the relation to  $(t_s, h_s) \in S$  explicit. Let  $C \neq \emptyset$ . Then a.s. for  $n$  large enough it is

$$\max_{(t_s, h_s) \in S \setminus R} \left( \min\{|\hat{t}_{e_s}^{(n)} - c_u| : c_u \in C\} \right) \leq \delta - 1, \quad (25)$$

i.e., all potential paths that start in the 'upper part'  $S \setminus R$  of  $\Delta_\delta$  end close to a  $c_u \in C$ . (25) holds true, as for any  $(t_s, h_s) \in S \setminus R$  the path eventually enters an  $A_u$  and then Proposition 4.3 states a.s.  $|\hat{t}_{e_s}^{(n)} - c_u| \leq \delta - 1$  for  $n$  large. The maximum follows from  $|S|$  being finite. Further, a.s. for  $n$  large it is

$$\min_{(t_s, h_s) \in \bigcup_{u=1, \dots, |C|} A_u} [(nh)^{-1/2} \cdot |D_{t,h}^{(n)}|] > \max_{(t_s, h_s) \in R} [(nh)^{-1/2} \cdot |D_{t,h}^{(n)}|], \quad (26)$$

i.e., as long as the algorithm does not break, starting points are first chosen from  $S \setminus R \supset \bigcup_u A_u$  up until all of them are cut out, and after that they are chosen from  $R$ . (26) follows from Corollary 3.2 and Lemma 3.3, noting that  $d_{t,h}^{(1)} = 0$  if  $(t, h) \in R$ , and  $|d_{t,h}^{(1)}| > 0$  if  $(t, h) \in A_u$ .

Combining (25) and (26), it follows that a.s. for  $n$  large at first all  $c \in C$  are estimated up to a distance  $\delta - 1$  from starting values within  $S \setminus R$ , given the algorithm does not break. Possibly step 3a is applied in between. We need to show that the breaking criterion 3b applies appropriately: First, for  $m \leq |C|$  we show that it does not apply. A path starting in  $S \setminus R$  must pass an  $A_u$  such that a.s. for  $n$  large

$$\min_{(t_s, h_s) \in S \setminus R} \left[ \max_{k=0, 1, \dots, h_s - \delta} |D_{\hat{t}_s^{(n)}(k), h_s - k}^{(n)}| \right] \geq \min_{(t, h) \in \bigcup_u A_u} |D_{t,h}^{(n)}| > n^\beta,$$

i.e., the maximum w.r.t. any path starting in  $S \setminus R$  exceeds the minimum w.r.t. to all  $A_u$ , and the second inequality holds as  $D_{t,h}^{(n)} = n^{1/2}d_{t,h}^{(1)} + o_{a.s.}(n^{1/2})$  uniformly on  $\Delta_\delta$  (Corollary 3.2) and  $|d_{t,h}^{(1)}| > 0$  within all  $A_u$  (Lemma 3.3), noting that  $\beta < 1/2$ . Thus, a.s. for  $n$  large there is no break.

Second, for  $m = |C| + 1$  the algorithm now breaks. All  $c \in C$  are estimated. Thus, possibly after applying criterion 3a, all remaining starting points lie in  $R$ . This also covers  $C = \emptyset$ . Note that a path that starts in  $R$  remains in  $R$ . It holds a.s. for  $n$  large

$$\max_{(t_s, h_s) \in R} \left[ \max_{k=0,1,\dots, h_s-\delta} |D_{\hat{t}_s^{(n)}(k), h_s-k}^{(n)}| \right] \leq \max_{(t,h) \in R} |D_{t,h}^{(n)}| < n^{1/2-v},$$

i.e., the maximum w.r.t. all paths starting in  $R$  exceeds the maximum w.r.t. the entire  $R$ . For the second inequality we note that within  $R$  it is  $d_{t,h}^{(1)} = 0$  and thus  $D_{t,h}^{(n)} = o_{a.s.}(n^{1/2-v})$  uniformly on  $R$  (Corollary 3.2). As  $\beta \geq 1/2 - v$ , a.s. for  $n$  large the algorithm breaks.

Finally note that 3c. is asymptotically redundant: a.s. for  $n$  large, for  $m \leq |C|$  we stated correct estimation up to the error, so neighboring estimates will have at least distance  $\delta_C - 2(\delta - 1)$ , and for  $m = |C| + 1$  the algorithm already broke in 3b.  $\square$

## References

- Antoch, J. and Hušková, M. (1999). Estimators of changes. In Asymptotics, nonparametrics, and time series, volume 158 of Statist. Textbooks Monogr., pages 533–577. Dekker, New York.
- Aston, J. A. D. and Kirch, C. (2012). Evaluating stationarity via change-point alternatives with applications to fmri data. Ann. Appl. Stat., 6(4):1906–1948.
- Berkes, I., Horváth, L., Kokoszka, P., and Shao, Q.-M. (2006). On discriminating between long-range dependence and changes in mean. Ann. Statist., 34(3):1140–1165.
- Brodsky, B. (2017). Change-point analysis in nonstationary stochastic models. CRC Press, Boca Raton, FL.
- Chen, J. and Gupta, A. K. (2000). Parametric statistical change point analysis. Birkhäuser Boston, Inc., Boston, MA.
- Cho, H. and Kirch, C. (2020). Two-stage data segmentation permitting multiscale change points, heavy tails and dependence.
- Chu, C.-S. J., Hornik, K., and Kuan, C.-M. (1995). MOSUM tests for parameter constancy. Biometrika, 82(3):603–617.
- Csörgő, M. and Horváth, L. (1997). Limit theorems in change-point analysis. Wiley Series in Probability and Statistics. John Wiley & Sons, Ltd., Chichester. With a foreword by David Kendall.
- Dehling, H., Rooch, A., and Taqqu, M. S. (2017). Power of change-point tests for long-range dependent data. Electron. J. Stat., 11(1):2168–2198.
- Döring, M. (2010). Multiple change-point estimation with  $U$ -statistics. J. Statist. Plann. Inference, 140(7):2003–2017.
- Eichinger, B. and Kirch, C. (2018). A mosum procedure for the estimation of multiple random change points. Bernoulli, 24(1):526–564.

- Fang, X., Li, J., and Siegmund, D. (2020). Segmentation and estimation of change-point models: false positive control and confidence regions. Ann. Statist., 48(3):1615–1647.
- Fryzlewicz, P. (2014). Wild binary segmentation for multiple change-point-detection. Ann Stat, 42(6):2243–2281.
- Gombay, E. and Horváth, L. (1994). An application of the maximum likelihood test to the change-point problem. Stochastic Process. Appl., 50(1):161–171.
- Gombay, E. and Horváth, L. (2002). Rates of convergence for  $U$ -statistic processes and their bootstrapped versions. volume 102, pages 247–272. Silver jubilee issue.
- Harchaoui, Z. and Lévy-Leduc, C. (2010). Multiple change-point estimation with a total variation penalty. J. Amer. Statist. Assoc., 105(492):1480–1493.
- Hinkley, D. V. (1971). Inference about the change-point from cumulative sum tests. Biometrika, 58:509–523.
- Holmes, M., Kojadinovic, I., and Quessy, J.-F. (2013). Nonparametric tests for change-point detection à la Gombay and Horváth. J. Multivariate Anal., 115:16–32.
- Horváth, L. and Hušková, M. (2005). Testing for changes using permutations of  $U$ -statistics. J. Statist. Plann. Inference, 128(2):351–371.
- Horváth, L. and Shao, Q.-M. (2007). Limit theorems for permutations of empirical processes with applications to change point analysis. Stochastic Process. Appl., 117(12):1870–1888.
- Hušková, M. and Slabý, A. (2001). Permutation tests for multiple changes. Kybernetika (Prague), 37(5):605–622.
- Kass-Hout, T., Xu, Z., McMurray, P., Park, S., Buckeridge, D., Brownstein, J., Finelli, L., and Groseclose, S. (2012). Application of change point analysis to daily influenza-like illness emergency department visits. Journal of the American Medical Informatics Association : JAMIA, 19:1075–81.
- Killick, R., Eckley, I. A., Ewans, K., and Jonathan, P. (2010). Detection of changes in variance of oceanographic time-series using changepoint analysis. Ocean Engineering, 37(13):1120 – 1126.
- Lavielle, M. and Moulines, E. (2000). Least-squares estimation of an unknown number of shifts in a time series. J. Time Ser. Anal., 21(1):33–59.
- Levajkovic, T. and Messer, M. (2021). mscp: Multiscale Change Point Detection via Gradual Bandwidth Adjustment in Moving Sum Processes. R package version 1.0.
- Matteson, D. S. and James, N. A. (2014). A nonparametric approach for multiple change point analysis of multivariate data. J Am Stat Assoc, 109(505):334–345.
- Messer, M. (2019). Bivariate change point detection: joint detection of changes in expectation and variance.
- Messer, M., Kirchner, M., Schiemann, J., Roeper, J., Neining, R., and Schneider, G. (2014). A multiple filter test for the detection of rate changes in renewal processes with varying variance. Ann. Appl. Stat., 8(4):2027–2067.
- Ministry of Health and Child Care of Zimbabwe (2021). Historical data on the daily number of new reported covid-19 cases in Zimbabwe. pages Sources accessed 25. February 2021, [http://www.mohcc.gov.zw/index.php?option=com\\_content&view=category&layout=blog&id=84&Itemid=435](http://www.mohcc.gov.zw/index.php?option=com_content&view=category&layout=blog&id=84&Itemid=435).

- Page, E. S. (1954). Continuous inspection schemes. Biometrika, 41:100–115.
- Pein, F., Sieling, H., and Munk, A. (2017). Heterogeneous change point inference. J R Stat Soc Series B Stat Methodol, 79(4):1207–1227.
- Reeves, J., Chen, J., Wang, X. L., Lund, R., and Lu, Q. Q. (01 Jun. 2007). A review and comparison of changepoint detection techniques for climate data. Journal of Applied Meteorology and Climatology, 46(6):900 – 915.
- Rybach, D., Gollan, C., Schluter, R., and Ney, H. (2009). Audio segmentation for speech recognition using segment features. In 2009 IEEE International Conference on Acoustics, Speech and Signal Processing, pages 4197–4200.
- Spokoiny, V. (2009). Multiscale local change point detection with applications to value-at-risk. Ann. Statist., 37(3):1405–1436.
- Steinebach, J. and Eastwood, V. R. (1995). On extreme value asymptotics for increments of renewal processes. volume 45, pages 301–312. Extreme value theory and applications (Villeneuve d’Ascq, 1992).

## Contact information

Tijana Levajković

email.: [tijana.levajkovic@tuwien.ac.at](mailto:tijana.levajkovic@tuwien.ac.at)

Michael Messer

email.: [michael.messer@tuwien.ac.at](mailto:michael.messer@tuwien.ac.at)

Vienna University of Technology

Institute of Statistics and Mathematical Methods in Economics

Wiedner Hauptstraße 8-10/105

1040 Vienna, Austria